Translatome of dorsal striatum parvalbumin interneurons revisited: insights across diverse experimental paradigms

Claire Naon, Laia Castell, Steeve Thirard, Maria Moreno, Stéphanie Rialle, Eva Goetz, Eloi Casals, Angelina Rogliardo, Marta Gut, Anna Esteve-Codina, et al.

frontiers | Frontiers in Cellular Neuroscience

TYPE Original Research
PUBLISHED 15 October 2025
DOI 10.3389/fncel.2025.1648461

OPEN ACCESS

EDITED BY
Elodie Fino,
INSERM U901 Institut de Neurobiologie de la Méditerranée, France

REVIEWED BY
Jenesis Kozel,
University of Pittsburgh, United States
Michel Engeln,
University of Bordeaux, France

*CORRESPONDENCE
Emmanuel Valjent
✉ emmanuel.valjent@gmail.com;
✉ emmanuel.valjent@inserm.fr

†These authors have contributed equally to this work

RECEIVED 17 June 2025
ACCEPTED 27 August 2025
PUBLISHED 15 October 2025

CITATION
Naon C, Castell L, Thirard S, Moreno M, Rialle S, Goetz E, Casals E, Rogliardo A, Gut M, Esteve-Codina A, Quintana A, Bertaso F, Valjent E and Cutando L (2025) Translatome of dorsal striatum parvalbumin interneurons revisited: insights across diverse experimental paradigms.
Front. Cell. Neurosci. 19:1648461.
doi: 10.3389/fncel.2025.1648461

Translatome of dorsal striatum parvalbumin interneurons revisited: insights across diverse experimental paradigms

Claire Naon[1†], Laia Castell[2†], Steeve Thirard[3], Maria Moreno[3], Stéphanie Rialle[4], Eva Goetz[1], Eloi Casals[5,6], Angelina Rogliardo[1], Marta Gut[5,6], Anna Esteve-Codina[5,6], Albert Quintana[7,8], Federica Bertaso[1], Emmanuel Valjent[1*†] and Laura Cutando[7,8†]

[1]INM, University Montpellier, Inserm, Montpellier, France, [2]Department of Neuroscience, Northwestern University Feinberg School of Medicine, Chicago, IL, United States, [3]IGF, University Montpellier, CNRS, Inserm, Montpellier, France, [4]MGX-Montpellier GenomiX, University Montpellier, CNRS, Inserm, Montpellier, France, [5]Centro Nacional de Análisis Genómico (CNAG), Barcelona, Spain, [6]Universitat de Barcelona (UB), Barcelona, Spain, [7]Institut de Neurociències, Universitat Autònoma de Barcelona, Bellaterra, Spain, [8]Departament de Biologia Cellular, Fisiologia i Immunologia, Universitat Autònoma de Barcelona, Barcelona, Spain

Parvalbumin (PV) interneurons in the dorsal striatum (DS) are fast-spiking GABAergic cells critical for feedforward inhibition and synaptic integration within basal ganglia circuits. Despite their well-characterized electrophysiological roles, their molecular identity remains incompletely defined. Using the Ribotag approach in *Pvalb-Cre* mice, we profiled the translatome of DS PV interneurons and identified over 2,700 transcripts significantly enriched (fold-change > 1.5) in this population. Our data validate established PV markers and reveal a distinct molecular signature of DS PV neurons compared to PV interneurons from the nucleus accumbens. Gene ontology analyses highlight prominent expression of genes related to extracellular matrix components, cell adhesion molecules, synaptic organization, ion channels, and neurotransmitter receptors, particularly those mediating glutamatergic and GABAergic signaling. Notably, perineuronal net markers were robustly expressed in DS PV interneurons and confirmed by immunofluorescence. Transcriptomic analysis of DS PV neurons following repeated d-amphetamine exposure identified *Gm20683* as the only differentially expressed transcript between treated groups. Furthermore, RNAseq analysis of mice subjected to an operant behavior paradigm with two types of food reward (high-palatable diet or standard chow) identified over 1,000 and 100 genes enriched in DS PV neurons from standard and high-palatable masters, respectively. These findings provide a comprehensive molecular profile of DS PV interneurons, distinguishing them from other striatal PV populations, and reveal specific gene expression changes associated with psychostimulant exposure and reward-driven behaviors. Our findings deepen insight into the molecular mechanisms of PV interneuron activity in striatal circuits and their potential roles in neuropsychiatric, motor and reward-related disorders.

KEYWORDS

striatum, interneurons, parvalbumin, translatome, food-seeking behavior

Introduction

The striatum, the primary input nucleus of the basal ganglia, is classically categorized into dorsal and ventral compartments. The dorsal striatum (DS) receives converging excitatory inputs from both the cortex and the thalamus (Graybiel and Grafton, 2015; Hintiryan et al., 2016; Hunnicutt et al., 2016; Pan et al., 2010; Smith and Bolam, 1990; Tisch et al., 2004). These inputs are subsequently processed and converted into an inhibitory signal projecting toward the basal ganglia output nuclei. Based on the targeted output regions, two main GABAergic projection pathways are typically described: the striatonigral (direct) pathway, which projects to the substantia nigra pars reticula (SNr) and the internal pallidum (GPi), and the striatopallidal (indirect) pathway, which projects to the external pallidum (GPe) (Oh et al., 2014). The direct and indirect striatal projection neurons (dSPNs and iSPNs) define these downstream pathways, respectively, (Gerfen et al., 2013; Kreitzer and Malenka, 2008; Marsden and Obeso, 1994). SPNs constitute approximately 95% of all striatal neurons (Tisch et al., 2004), the remaining 5% being interneurons that form a highly organized and hierarchical network, essential for efficient input processing and proper striatum function (Graveland and DiFiglia, 1985; Tepper et al., 2018).

The population of dorsal striatal interneurons can be classified into either cholinergic or GABAergic subtypes which comprise four major classes based on their molecular and firing properties. These clusters include interneurons expressing parvalbumin (PV), neuropeptide Y, tyrosine hydroxylase and calretinin (Kreitzer, 2009; Tepper et al., 2018; Tepper and Bolam, 2004). Among them, PV interneurons, also described as fast-spiking interneurons (FSIs), represent the main population of GABAergic interneurons (Tepper et al., 2018). By receiving converging excitatory inputs, they mediate rapid feedforward inhibition of SPNs, thereby modulating the striatal plasticity necessary for the proper integration of excitatory information by SPNs (Arias-García et al., 2018; Choi et al., 2019; Duhne et al., 2021; Gage et al., 2010; Gittis et al., 2010; Mallet et al., 2005; Owen et al., 2018; Planert et al., 2013; Roberts et al., 2019; Sciamanna et al., 2015; Tepper and Bolam, 2004). Importantly, disruption of PV activity has been associated with core motor symptoms of neurological and neurodevelopmental disorders including obsessive-compulsive disorder (OCD), dyskinesias, Tourette syndrome, motor stereotypies in autism spectrum disorder (ASD) and schizophrenia (Burguière et al., 2013; Gittis et al., 2011; Mondragón-González et al., 2024; Zhou et al., 2021). Moreover, the requirement of PV interneurons of the ventral striatum/nucleus accumbens (Acb) seems crucial in the addictive-like behaviors induced by psychostimulant exposure such as amphetamine and cocaine (Gallegos et al., 2023; Manz et al., 2022; Wang et al., 2018), which may highlight a more global role of PV interneurons in reward learning and conditioning (Hazlett et al., 2024; Lee et al., 2018; Yamada et al., 2016). Nevertheless, studies specifically addressing DS PV interneurons in the context of psychostimulant exposure and reward circuitry are lacking (Todtenkopf et al., 2004). Surprisingly, although DS PV interneurons have been extensively studied at the functional level, insight related to their molecular profile remain limited to a restricted number of genes identified using single-cell transcriptomic (Muñoz-Manchado et al., 2018; Saunders et al., 2018). The present study aimed to establish the translatome of DS PV interneurons using the Ribotag approach, allowing cell type-specific gene expression profiling (Puighermanal et al., 2020; Sanz et al., 2009). We generated *Pvalb-Ribotag* mice and identified over 2.700 transcripts enriched in DS PV interneurons. Additionally, we investigated whether repeated exposure to d-amphetamine, as well as, food-seeking behaviors (standard vs. high palatable food) and contingency (master vs. yoked mice) impacted gene expression in DS PV interneurons.

Materials and methods

Animals

All animal procedures were conducted in accordance with the guidelines of the French Agriculture and Forestry Ministry for handling animals (authorization number/license B34-172-41) and approved by the relevant local and national ethics committees (authorization APAFIS#38912). Female and male mice were used for all experiments. Animals were housed in groups of 2 to 5 per cage under standardized conditions with a 12-h light/dark cycle, *ad libitum* food and water, stable temperature (22 ± 2°C) and controlled humidity (55 ± 10%). The mouse models used in this study were derived from the following original strains: *Pvalb*-IRES-Cre/+ (B6.129P2-*Pvalb*$^{tm1(cre)Arbr}$/J, RRID: IMSR_JAX:017320), Ribotag (B6J.129(Cg)-*Rpl22*$^{tm1.1Psam}$/SjJ, RRID: IMSR_JAX:029977), Ai14 (B6;129S6-*Gt(ROSA)26Sor*$^{tm14(CAG-tdTomato)Hze}$/J), Ai32 (B6;129S-*Gt(ROSA)26Sor*$^{tm32(CAG-COP4*H134R/EYFP)Hze}$/J). To generate *Pvalb*-reporter mice, *Pvalb*-IRES-Cre/+ mouse line was crossed with the Ribotag line to generate *Pvalb-Ribotag* mice, with the Ai32 line (which express an improved channelrhodopsin-2/EYFP fusion protein) to generate *Pvalb-ChR2* mice, with the Ai14 line to generate *Pvalb-Ai14* mice, and with the Ai32; Ribotag line to generate *Pvalb-ChR2-Ribotag* mice.

Mouse strains used for immunofluorescence included *Pvalb-ChR2-Ribotag* mice ($n = 2$), *Pvalb-ChR2* mice ($n = 3$), *Pvalb-Ribotag* mice ($n = 4$) and *Pvalb-Ai14* mice ($n = 3$). *Pvalb-Ribotag* mice were used for low-input RNA-sequencing (RNA-seq). The experimental groups included: saline ($n = 7$), D-amphetamine ($n = 8$), highly palatable food master ($n = 6$), highly palatable food yoked ($n = 6$), standard food master ($n = 6$), and standard food yoked ($n = 6$). For each RNAseq sample, striatal tissue from two to three mice were pooled.

Drugs and treatments

(+)-α-Methylphenethylamine [D-amphetamine (D-amph)] sulfate salt (5 mg/kg) from Tocris was dissolved in 0.9% (w/v) NaCl (saline) and injected intraperitoneally (i.p) in a volume of 10 mL/kg. Mice were administered with d-amphetamine (5 mg/kg) during 5 days and euthanized 3 days after the last injection.

Immunofluorescence

Free-floating sections (30 µm) of the dorsal striatum were prepared as previously described (Cutando et al., 2021). On day 1, slices were washed for 10 min in PBS (3x), incubated 15 min in 0.2% Triton X-100 in PBS before incubation overnight at 4°C with primary antibodies including chicken anti-GFP (1:500, Invitrogen, #A10262),

rat anti-HA (1:500, Roche, #11867431001), goat anti-PV (1:500, Swant, #PVG-213), rabbit anti-PV (1:1000, Swant, #PV25), mouse anti-RFP (1:1,000, MBL, #M155-3), rabbit anti-TTF1 (1:500, Santa-Cruz, #sc-13040) and N-acetylgalactosamine-binding Wisteria floribunda agglutinin (WFA, 1:1000, Sigma, #L1516). Non-specific binding was blocked with 10% Normal Donkey Serum (NDS) in PBS for 2 h for WFA staining. On day 2, slices were rinsed in PBS and incubated 45 min with various combination of the following secondary antibodies: goat Alexa Fluor 488-coupled anti-chicken (1:500, Jackson ImmunoResearch, #103-545-155), donkey Alexa Fluor 488-coupled anti-goat (1:500, Jackson ImmunoResearch, #103-545-003), donkey Alexa Fluor 647-coupled anti-goat (1:500, Jackson ImmunoResearch, #103-605-003), donkey Alexa Fluor 594-coupled anti-mouse (1:500, Jackson ImmunoResearch, #103-585-150), goat Alexa Fluor 594-coupled anti-mouse (1:500, Jackson ImmunoResearch, #103-585-003), goat Alexa Fluor 488-coupled anti-rabbit (1:500, Invitrogen, #A11034), goat Cy3-coupled anti-rabbit (1:500, Jackson ImmunoResearch, #111-165-003), donkey Alexa Fluor 647-coupled anti-rat (1:500, Jackson ImmunoResearch, #712-605-150), goat Alexa Fluor 647-coupled anti-rat (1:500, Thermo Fisher Cat#112-005-003) and Streptavidin A488 (1:500, Invitrogen, #S11223) or Streptavidin Atto 550 (1500, Sigma, #96404). Sections were then rinsed twice in PBS before mounting on SuperFrost® slides (VWR #631-0108) and coverslipped with a xylene-based mounting medium (Leica Micromount #3801731). Slices were stored at 4°C until imaging. Confocal miscroscopy/imaging were carried out at the Montpellier RIO Imaging Facility. Fluorescent images of labeled cells in the region of interest were captured using sequential laser scanning confocal microscopy (Leica SP8). Three to eight images per hemisphere from four to six sections for a given marker were used for quantifications. Adjacent serial sections were never counted for the same marker to avoid any potential double counting of hemisected neurons. Images have been analyzed using Fiji software.

Tissue collection for polyribosome immunoprecipitation

Whole striata were extracted from adult *Pvalb-Ribotag* mice, as previously described (Puighermanal et al., 2020). Mice chronically treated with d-amph (5 mg/kg) or saline were sacrificed 3 days after the last administration. Mice that underwent the operant behavior task were euthanized 1 day after the last FR5 training session. Striatal tissue from two to three mice was pooled to generate a single sample for polyribosome immunoprecipitation and subsequent RNAseq.

Polyribosome immunoprecipitation

HA-tagged ribosome cell-type-specific mRNA purification by Translating Ribosome Affinity Purification (TRAP) from striatal samples of *Pvalb-Ribotag* mice was performed as previously described (Cutando et al., 2022), using 5 µL of anti-HA antibody (Clone 16B12; BioLegend, 901513) and magnetic beads (Fisher Scientific, #88803). Total RNA from the pellet fractions was extracted using the RNeasy Micro Kit (Qiagen, #73934), and from the input fractions using the RNeasy Mini Kit (Qiagen, #74104), following the manufacturer's instructions. An on-column DNase treatment was included to eliminate genomic DNA contamination. RNA quality and quantity were assessed using 1 µL of sample on a Nanodrop One spectrophotometer (Thermo Scientific). For the translatome profile experiment, three biological replicates were used for the RNAseq analysis, each consisting of pooled tissue from 2 to 3 mice. For the d-amphetamine experiment, three biological replicates were used, each consisting of pooled tissue from 2 to 3 mice. For the operant behavior experiment, two biological replicates were used per group, each consisting of pooled striata from 2 to 3 mice.

Low-input RNA sequencing and data processing

RNA sequencing libraries from *Pvalb-Ribotag* mice striatal tissue were prepared following the SMART-seq2 protocol (Picelli et al., 2014), with some modifications. Briefly, total RNA samples were quantified using the Qubit® RNA BR Assay Kit (Thermo Fisher Scientific), and RNA integrity was assessed with the Agilent DNF-471 RNA (15 nt) Kit on the Fragment Analyzer 5,200 system (Agilent). Reverse transcription was performed on 1.8 µL of total RNA input (6–11 ng, depending on sample availability) using SuperScript II (Invitrogen) in the presence of oligo-dT30VN primers (1 µM; 5′-AAGCAGTGGTATCAACGCAGAGTACT30VN-3′), template-switching oligonucleotides (1 µM), and betaine (1 M). The resulting cDNA was amplified using KAPA HiFi HotStart ReadyMix (2×) (Roche) and 100 nM IS PCR primer (5′-AAGCAGTGGTATCAACGCAGAGT-3′), with 8 cycles of PCR. After purification with Agencourt AMPure XP beads (1:1 ratio; Beckman Coulter), product size distribution and concentration were evaluated using the Bioanalyzer High Sensitivity DNA Kit (Agilent). A total of 200 ng of amplified cDNA was fragmented for 10 min at 55°C using the Nextera XT Kit (Illumina), followed by 12 cycles of amplification with indexed Nextera PCR primers. The resulting libraries were purified twice using Agencourt AMPure XP beads (0.8:1 ratio) and quantified again using the Bioanalyzer High Sensitivity DNA Kit. Sequencing was performed on an Illumina NovaSeq 6000 system in paired-end mode with a read length of 2 × 51 bp, according to the manufacturer's protocol for dual indexing. Image analysis, base calling, and quality scoring were carried out using Real Time Analysis (RTA) software version 3.4.4, followed by the generation of FASTQ files.

For the operant behavior experiment (Figure 1), RNA-seq reads were mapped against the *Mus musculus* genome (GRCm38) using STAR 2.5.3a (Dobin et al., 2013) with ENCODE parameters. Gene-level quantification was performed with RSEM 1.3.0 (Li and Dewey, 2011) using the gencode. M21 annotation. For the d-amphetamine experiment (Figure 1), RNAseq reads were aligned against the *Mus musculus* genome (GRCm39) using STAR 2.7.8a (Dobin et al., 2013), also with ENCODE parameters and gene quantification was performed with RSEM 1.3.0 (Dobin et al., 2013) using the gencode. M34 annotation.

RNAseq differential expression

Genes with at least 1 count-per-million reads (cpm) in at least 3 samples were retained. Counts were normalized using the trimmed

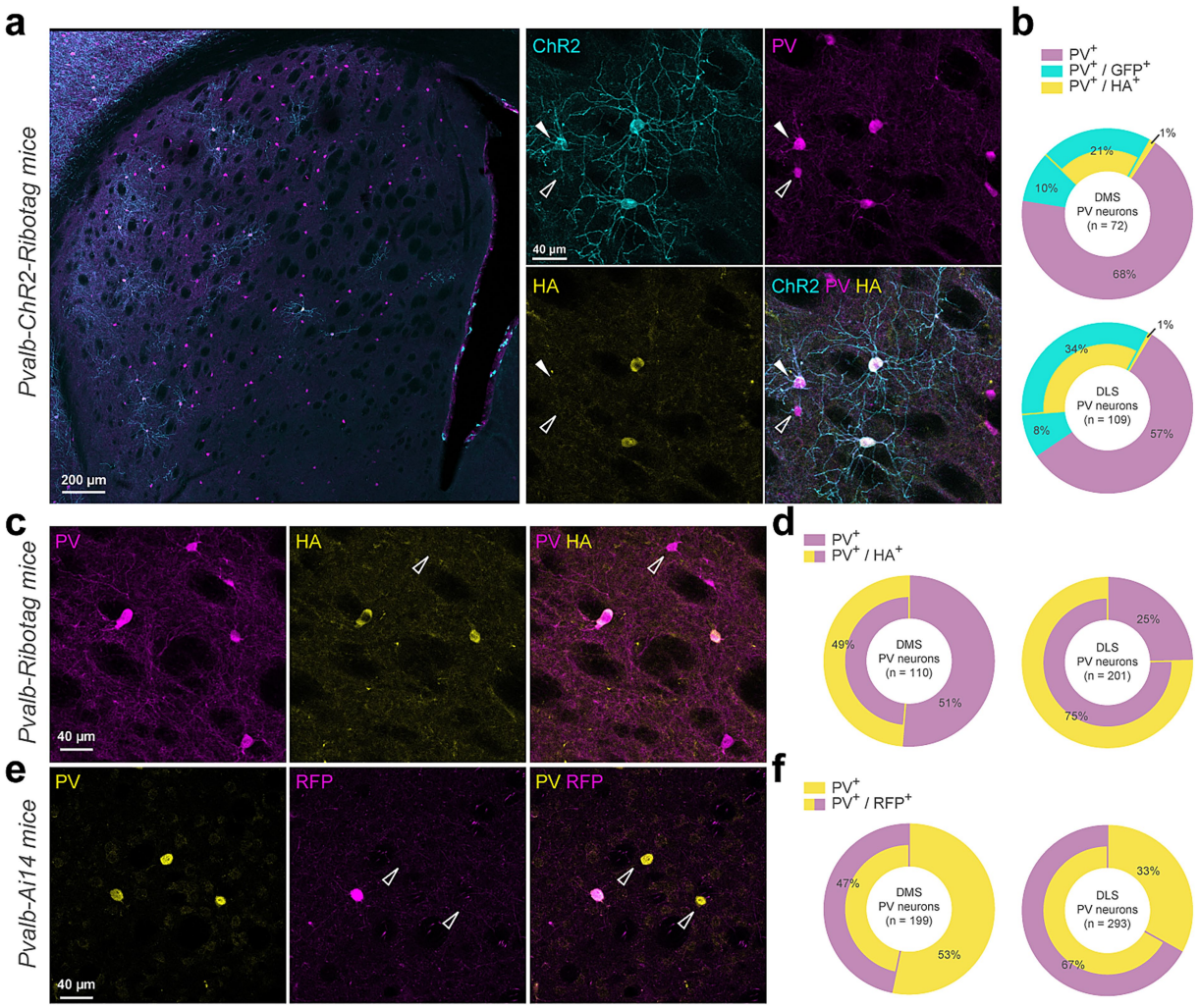

FIGURE 1
Cre-dependent report proteins expression is restrained to a subpopulation of Parvalbumin-positive interneurons. **(a)** Coronal striatal section from a *Pvalb-ChR2-Ribotag* mouse showing GFP reporter fluorescence (cyan) and stained with PV (magenta), HA (yellow). **(b)** Doughnut charts summarize the proportion of cells expressing either parvalbumin alone (PV+) or combinations of PV+, GFP+ and/or HA+ markers. **(c)** Immunostaining of a *Pvalb-Ribotag* striatal section for PV (magenta) and HA (yellow) and **(d)** summary data for simple (PV+) or double stained (PV+/HA+) neurons. **(e)** Immunostaining of a *Pvalb-Ai14* striatal section for PV (yellow) and RFP (magenta) and **(f)** summary data for simple (PV+) or double stained (PV+/RFP+) neurons.

mean of M-values (TMM) method and transformed into log2-counts per million (logCPM). Differential gene expression analysis was performed using the limma R package v3.54.2 (Ritchie et al., 2015). The voom function (Law et al., 2014) was used to estimate the mean–variance relationship and compute observation-level weights. These voom-transformed counts were used to fit linear models. Functional enrichment analysis was conducted using g: Profiler via the gprofiler2 R package v0.1.8 (Kolberg et al., 2023) and ShinyGO (Ge et al., 2020). Multidimensional scaling plots were generated with the limma function plotMDS using the top 500 most variable genes.

Behaviors

Locomotor response to d-amphetamine

Mice were tested in a circular corridor system (Imetronic, Pessac, France) for 120 min. Horizontal activity was recorded when mice triggered two adjacent infrared beams positioned 1 cm above the floor in each 90° section of the corridor, indicating movement through one-quarter of the circular track. Vertical activity, measured as rearing, was recorded when mice broke beams placed 7.5 cm above the floor, reflecting upright exploratory movements. Prior to drug administration, *Pvalb-Ribotag* mice underwent a two-day habituation period. Each day, they were placed in the activity chamber for 30 min, injected with saline, and then returned to the chamber for an additional 90 min. The following days, the same protocol was followed, with the exception that the mice were allocated to two groups: one administered with saline and the other with d-amphetamine (5 mg/kg, i.p.). This paradigm was repeated for five consecutive days.

Operant behavior

One week prior the experiments, mice were individually housed. Five days before conditioning, they were food-restricted to maintain

85% of their original body weight. Food restriction was maintained from day 1 to day 9, after which mice had *ad libitum* access to food from day 10 to day 15. Mice were assigned to one of two groups based on the type of food reward used in the operant paradigm. The high-palatable food group received isocaloric pellets (TestDiet) with the same caloric content as standard chow (3.48 kcal/g) but with a higher sucrose content (49% of carbohydrates) and chocolate flavoring. The standard food group received pellets with the same caloric and palatability profile as standard chow. The operant training began with a fixed ratio (FR)-1 schedule of reinforcement, during which mice were presented with two levers. Pressing the active lever resulted in the delivery of a pellet, while pressing the inactive lever had no consequences. Each reward delivery was followed by a 15-s time-out period, which was maintained throughout all experimental phases. Following the FR1 phase, mice underwent 4 days of FR5 training, where five presses on the active lever were required to receive a pellet. The final phase consisted of 6 additional days of FR5 training, during which mice had *ad libitum* access to food in their home cages. Within each food group, mice were further divided into master and yoked subgroups. Each yoked mouse was paired with a master mouse. Master mice performed the operant task as described, whereas yoked mice received a pellet passively whenever their paired master obtained a pellet. Lever presses by the yoked mice had no consequences.

Statistical analyses

Statistical analyses were performed with GraphPad Prism v10.4.0. Behaviors were analyzed with two-way repeated measure ANOVA or three-way ANOVA as detailed in Supplementary Table 4.

Results

Validation of the *Pvalb-Ribotag* mouse line reveals incomplete recombination

We first used *Pvalb-ChR2-Ribotag* mice to visualize PV interneurons and to confirm Ribotag recombination as co-expression of the HA tagged ribosomal subunit in PV + neurons. Triple immunofluorescence analyses revealed that endogenous PV interneurons identified using PV antibody outnumbered by far the ChR2-and/or HA-positive interneurons in the DS (Figures 1a,b). Indeed, no recombination was found in ~68% and ~57% of the PV interneurons analyzed in the dorsomedial (DMS) and dorsolateral striatum (DLS), respectively (Figure 1b). We also found a fraction of PV cells expressing either only ChR2 (DMS: ~10% and DLS: ~8%) or to a lesser extent expressing only HA (DMS: ~1% and DLS: ~1%) (Figures 1a,b). Facing this low rate of recombination, we decided to reevaluate the degree of recombination in two additional mouse lines, the *Pvalb-Ribotag* and the *Pvalb-Ai14* mice expressing the red fluorescent protein tdTomato (Figure 1c). In *Pvalb-Ribotag* mice, double immunofluorescence analyses revealed a higher percentage of PV interneurons expressing HA (Figures 1b,d). We also found that the percentage of PV/HA-expressing interneurons was higher in the DLS (~75%) compared to the DMS (~49%). Similar results were found when analyses were performed in *Pvalb-Ai14* mice in which ~67% and ~47% of the PV interneurons expressed RFP in the DLS and DMS, respectively (Figures 1e,f). Importantly, in none of the three mouse lines tested, did we detect cells expressing ChR2, HA or tdTomato in the ventral striatum.

Translatome profile of DS PV interneurons using *Pvalb-Ribotag* mice

The translatome of DS PV interneurons was established by identifying the relative enrichment of genes in the pellet fraction containing tagged Ribosomes-bound mRNAs compared to the input fraction where mRNAs from all cell types were present (Figure 2a). We first validated the selectivity of the approach by demonstrating the enrichment in the pellet fraction of well-established PV markers including *Pvalb, Cox6a2, Kcnc1, Vwc2, Clstn2, Nrip3, Nxph1, Pthlh, Ubash3b and Kcnip1* (Figure 2b; Supplementary Table 1) (Muñoz-Manchado et al., 2018; Saunders et al., 2018). Conversely, transcripts identifying spiny projection neurons (SPNs: *Gpr88, Ppp1r1b, Arpp19, Pde10a*) from both the direct (dSPNs: *Drd1, Pdyn, Tac1*, *Eya1*) and the indirect pathway (iSPNs: *Gpr6, Adora2a, Penk, Necab1*) (Gokce et al., 2016; Märtin et al., 2019) as well as other classes of striatal GABAergic interneurons (INs: *Npy, Sst, Htr3a, Calb2, Chodl*) and large cholinergic interneurons (CINs: *Chat, Slc17a8, Slc10a4, Ntrk1*) (Muñoz-Manchado et al., 2018) were all decreased (Figure 2c; Supplementary Table 1). Similar de-enrichment was found for genes used to classify astrocytes (*Gfap*, *Aldh1l1, S100b*), microglia (*Aif1*, *Trem2*, *Tmem119*) and oligodendrocytes (*Olig2*, *Cnp*, *Mog*) (Figure 2d). Among the 14,185 protein-coding genes detected in our RNAseq, 3,484 were identified as enriched in DS PV interneurons as compared to the DS inputs (adjusted p value of < 0.05) (Figure 2e; Supplementary Table 1). This number dropped down to 2,750 for those displaying a fold-change > 1.5 (Figure 2f; Supplementary Table 1). We also found a significant enrichment of several non-coding transcripts including 663 long non-coding RNAs (LncRNA), 963 To be Experimentally Confirmed RNAs (TEC) and 172 pseudogenes mainly composed of processed pseudogenes (147 out of 172) (Figure 2g; Supplementary Table 1).

Cross-analyses with previous single-cell RNAseq studies revealed that PV-enriched transcripts found in *Pvalb-Th-Pnoc* (Saunders et al., 2018) and *Pvalb-Pthlh* (Muñoz-Manchado et al., 2018) populations match at 55 and 62% with those identified in the present study (Figure 2h; Supplementary Table 1). We also compared the overlap between the genes we found to be enriched in the DS PV interneurons with those enriched in the PV interneurons of the nucleus accumbens (Acb) unveiled using the *Pvalb-Sun1-GFP* mouse line (Gallegos et al., 2023). *Pvalb-Sun1-GFP* mice express the nuclear envelope protein Sun1 fused to GFP specifically in PV-expressing neurons, enabling the isolation of nuclei and analysis of the nuclear transcriptome. In contrast, *Pvalb-Ribotag* mice express the ribosomal protein Rpl22 tagged with HA in PV neurons, allowing for the isolation of ribosome-associated, actively translated transcripts. Despite targeting distinct RNA populations, we identified 1,015 shared transcripts enriched between DS and Acb PV interneurons (Figure 2i; Supplementary Table 1). Among these common genes, 18 were found in the *Pvalb-Th-Pnoc* population and 30 in the *Pvalb-Pthlh* population (Figure 2j; Supplementary Table 1). All in all, only 4 transcripts (*Pvalb*, *Pthlh*, *Nxph1*, *Nrip3*) were found systematically enriched in PV

10.3389/fncel.2025.1648461

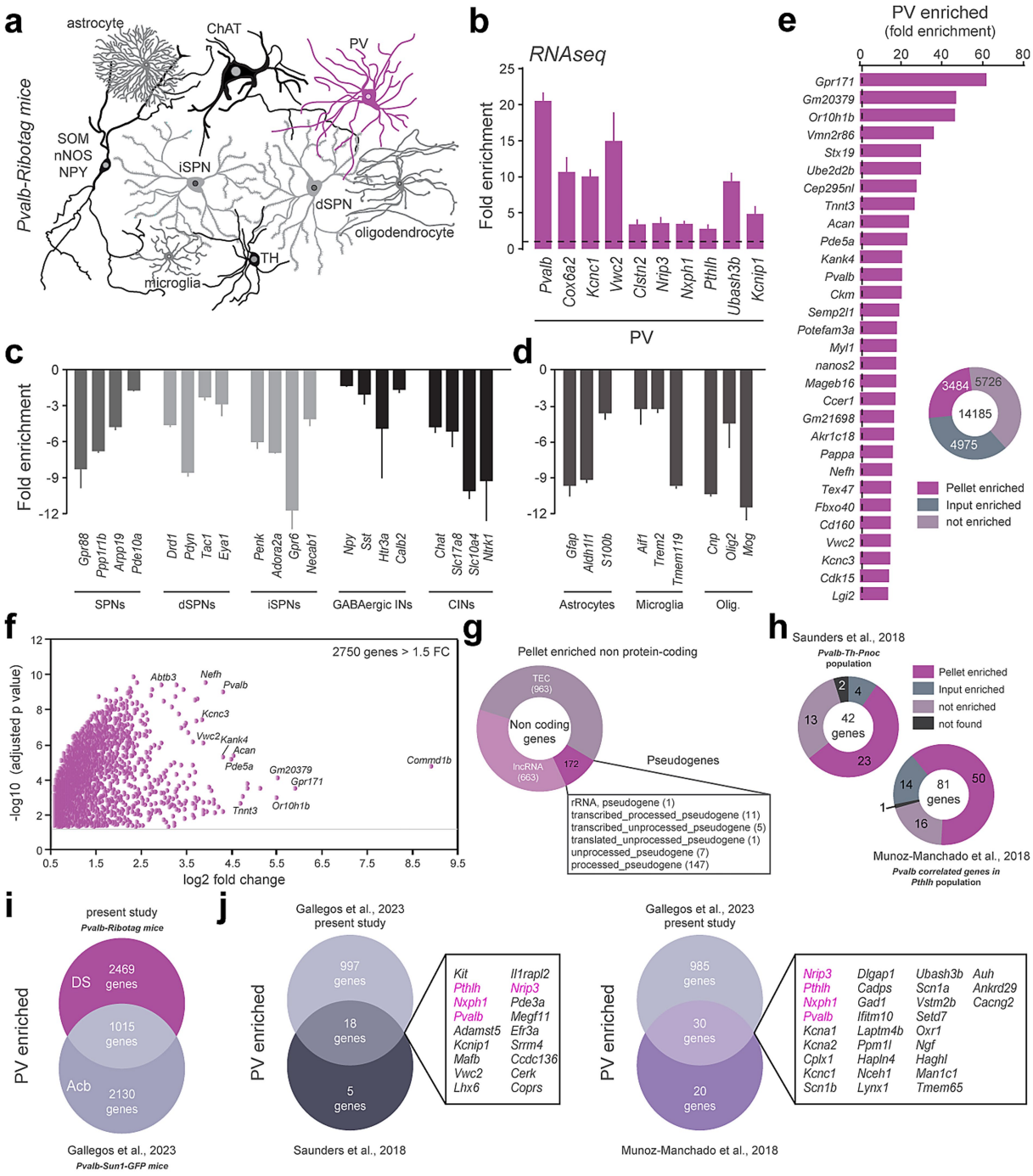

FIGURE 2
Translatome of PV-positive interneurons using the *Pvalb-Ribotag* mice. **(a)** Cartoon depicting the heterogeneity of striatal cell types. In magenta, the PV-positive cells targeted in *Pvalb-Ribotag* transgenic mice. **(b–d)** Validation by RNAseq of the enrichment of PV interneurons marker genes **(b)** and de-enrichment of markers for other striatal neurons **(c)** and other cell types **(d)** in the pellet fraction from HA-tag pull-down. **(e)** Protein-coding genes enrichment in the pellet fraction. **(f)** Volcano plot of protein-coding genes with a fold-change above 1.5 in the pellet fraction. **(g)** Doughnut plot of non-coding genes relative distribution according to subtypes: pseudogenes, TEC (To be Experimentally Confirmed) and long non-coding RNAs (lncRNA). **(h)** Proportion and number of PV-enriched transcripts previously identified using single cell RNAseq. **(i)** Venn diagram showing the number and overlap of genes enriched in PV interneurons in the dorsal striatum (DS) and nucleus accumbens (Acb). **(j)** Cross-comparison of genes identified in PV interneurons in mouse models from our and 3 different laboratories. The only 4 genes in common (*Pvalb*, *Pthlh*, *Nxph1*, *Nrip3*) are highlighted in purple.

interneurons regardless their location (DS vs. Acb) and the RNAseq approaches used (scRNAseq vs. TRAP) (Figure 2j; Supplementary Table 1). Finally, *in situ* hybridization from the Allen Brain Atlas dataset for *Nxph1*, *Nrip3*, *Laptm4b*, *Hmga1b* and *Setd7* transcripts presented a sparse distribution typical of DS PV interneurons (Supplementary Figure 1a).

Extracellular matrix and cell adhesion classification of DS PV interneurons

Gene Ontology (GO) enrichment analysis using the ShinyGO v0.8 web tool (Ge et al., 2020) revealed that synapse organization represented one of the most significant GO terms associated to Biological Process and Cellular Component (Supplementary Figure 2). Because synaptic stabilization is tightly associated with extracellular matrix (ECM) structures (Christensen et al., 2021; Wingert and Sorg, 2021), we examined whether ECM-related genes were enriched in DS PV interneurons using the MatrisomeDB database. Among 274 annotated core matrisome genes, we found transcripts encoding ECM glycoproteins (19), collagens (6) and proteoglycans (5) enriched in PV interneurons (Figure 3a; Supplementary Figure 3; Supplementary Table 2). We also identified several matrisome-associated genes among which some encode ECM regulators (22), ECM-affiliated proteins (12) and secreted factors (31) (Figure 3a; Supplementary Figure 3; Supplementary Table 2). Interestingly we noticed that 44 ECM-related genes enriched in DS PV interneurons were also found in Acb PV interneurons (labeled in magenta) (Figure 3a; Supplementary Table 2). Closed inspection of the identity of proteoglycan-enriched genes revealed the presence of core constituents of perineuronal nets (PNNs) including *Acan* and *Vcan* transcripts encoding for two chondroitin sulfate proteoglycans (Aggrecan and Versican) and *Hapln1* and *Hapln4* encoding for hyaluronan and proteoglycan link protein 1 and 4 (Figure 3a; Supplementary Table 2). To examine the presence of PNNs around DS PV interneurons, we performed *Wisteria floribunda* agglutinin (WFA) staining (Härtig et al., 2022) on striatal slices from *Pvalb-Ribotag* mice (Figure 3b), *Pvalb-ChR2* and *Pvalb*-Ai14 mice (Supplementary Figure 4) mice in which PV interneurons were identified indirectly with GFP, tdTomato or HA and directly using PV antibody. Immunofluorescence analysis revealed that regardless the mouse line and PV detection method used, PNNs ensheathe the majority of the DS PV interneurons, with WFA staining observed in more than 94% of them (Figure 3b; Supplementary Figure 4).

Cell adhesion molecules are also core constituents of synaptic organization and stabilization. We therefore analyzed the distribution of PV-enriched genes among cadherins, protocadherins, integrins as well as several different categories of cell adhesion molecules (Figure 3c; Supplementary Table 2). We found that genes encoding alpha isoforms of clustered protocadherins (9 out of 13: *Pcdhac1, Pcdhac2, Pcdha5, Pcdha6, Pcdha1, Pcdha2, Pcdha3, Pcdha7, Pcdha8*), non-clustered protocadherins (5 out of 12: *Pcdh7*, *Pcdh9, Pcdh10, Pcdh19, Pcdh15*), contactin-associated proteins (5 out 7: *Cntnap1*, *Cntnap4*, *Cntnap5c*, *Cntnap2*, *Cntnap5a*) as well as amigo (2 out of 3: *Amigo1*, *Amigo3*) or neurexin (2 out of 3: *Nrx2*, *Nrx3*) were particularly enriched in DS PV interneurons (Figure 3c; Supplementary Table 2). In contrast to ECM-related genes, only 17 cell adhesion-related genes were common to DS and Acb PV interneurons (labeled in magenta). These findings allow the identification of a unique ECM and adhesion molecule signature for DS PV interneurons (Figure 3c; Supplementary Table 2).

Neurotransmitter system and ion channels classification of DS PV interneurons

Cellular Component GO terms associated with synapses functions were also highly represented in our analysis (Supplementary Figure 2). We therefore took advantage of a system classification previously implemented allowing the rapid visualization of genes encoding receptors, transporters, and enzymes involved in the turnover of a given neurotransmitter system including serotonergic, catecholaminergic, GABAergic, cholinergic and glutamatergic (Puighermanal et al., 2020) (Figures 4a–e; Supplementary Table 3). These analyses revealed the enrichment of a restricted set of serotonergic (*Htr2b*, *Htr7*) (Figure 4a; Supplementary Table 3) and catecholaminergic (*Drd4*, *Adra1a*) receptors (Figure 4b). Several components of the GABAergic system were also found to be enriched including genes encoding GABAa and GABAb receptor subunits (*Gabra1*, *Gabrg3, Gabrd, Gabbr2*) as well as transcripts encoding proteins involved in GABA turnover (*Gad1*, *Gad2*) and transport (*Slc6a1*, *Slc6a8*) (Figure 4c; Supplementary Table 3). *Chrnb2* was the only cholinergic gene found to be enriched in DS PV interneurons (Figure 4d). Regarding the glutamatergic system, 10 out of the 18 genes encoding ionotropic glutamate receptors were enriched in PV interneurons (*Grik1, Grik3, Grik5, Gria3, Gria4, Grin1, Grin2a, Grin2b, Grin2d, Grid2*) while none of the transcripts encoding metabotropic glutamate receptors (*Grm*) were found to be enriched (Figure 4e; Supplementary Table 3). Finally, we found that DS and Acb PV interneurons only shared 5 neurotransmitter system-related genes, 3 associated to the GABAergic system (*Gabra1, Gad1, Slc6a8*) and 2 with the glutamatergic one (*Gria4, Grin2d*) (labeled in magenta) (Figure 4).

We also performed a complete classification of voltage-gated ion channels (Figure 5; Supplementary Table 3), including calcium channels (Figure 5a), sodium channels (Figure 5b), and potassium channels comprising voltage-gated potassium channels (Figure 5c), inwardly rectifying potassium channels (Figure 5d), two-P potassium channels (Figure 5e), calcium-activated potassium channels (Figure 5f), and accessory subunits (Figure 5g). The main pore-forming alpha 1 subunits of voltage-gated calcium channels were particularly enriched compared to the other subunits (7 out of 10 constituents) (Figure 5a). Voltage-gated potassium channels distributed among the different families were also highly enriched in DS PV interneurons, several of them displaying a fold-enrichment > 5 (*Kcna2, Kcnc1, Kcnc3, Kcng4, Kcnh2*) (Figure 5c). Our analysis also unveiled a biased expression in DS PV interneurons of G-protein activated inward rectifying potassium channels (*Kcnj3, Kcnj6, Kcnj9, Kcnj11, Kcnj12*) (Figure 5d). In contrast to neurotransmitter system-related genes, the expression of voltage-gated ion channels appears to be more conserved between DS and Acb PV interneurons as suggested by the important shared enriched expression of genes encoding voltage-gated potassium channels (9 out of 13 genes including *Kcna1, Kcna2, Kcnc1, Kcnc2, Kcnc3, Kcnb2, Kcng4, Kcns3, Kcnh2*) (Figure 5c), G-protein gated potassium channels (3 out of 5 genes: *Kcnj3, Kcnj9, Kcnj12*) (Figure 5d), Two-P potassium channels (*Kcnk3, Kcnk12*) and accessory subunits (3 out 3 genes: *Kcnab2, Kcnab3, Kcnmb2*) (Figure 5g).

Transcription factors classification of DS PV interneurons

Finally, to gain insights into the specification of DS PV interneurons, we classified transcription factors by family using the AnimalTFDB v4.0 database (Shen et al., 2023) (Supplementary Figure 5). We analyzed the distribution of DS PV

10.3389/fncel.2025.1648461

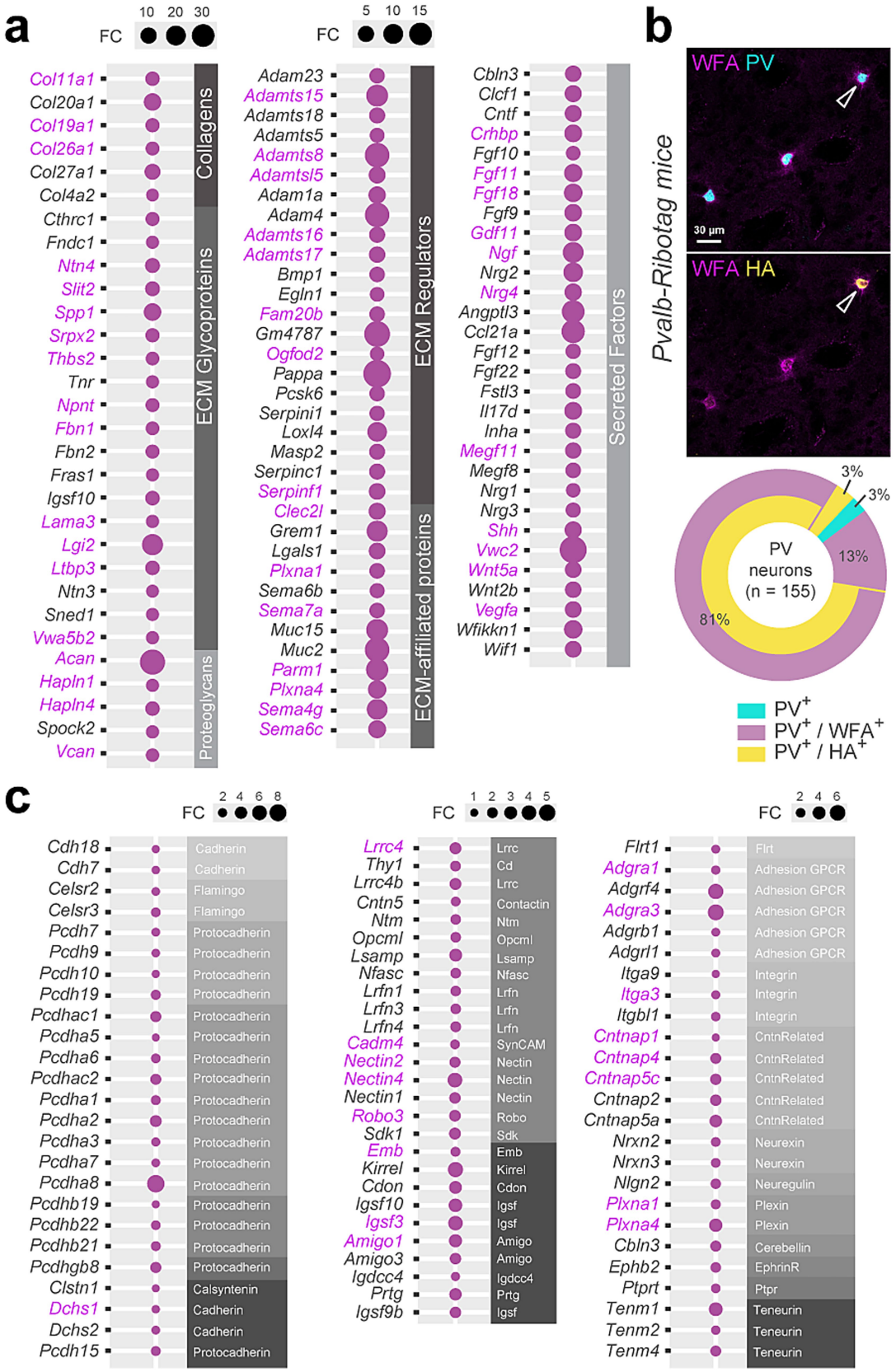

FIGURE 3
Molecular signature of DS PV interneurons transcripts related to extracellular components. **(a)** Extracellular matrix (ECM) genes enriched in DS PV interneurons, classified by sub-categories (gray bands). FC, fold change. Magenta, genes also enriched in Acb PV neurons **(b)** Perineuronal nets identified using *Wisteria floribunda* agglutinin (WFA) in *Pvalb-Ribotag* mice, highlighting the presence of ECM around the majority of PV-positive cells and only a minority of PV-negative cells. The Doughnut chart depicts the percentage of co-labeling for the different stainings. **(c)** Cell adhesion molecules transcripts enriched in DS PV interneurons. Enriched genes in common between DS and Acb are highlighted in magenta.

10.3389/fncel.2025.1648461

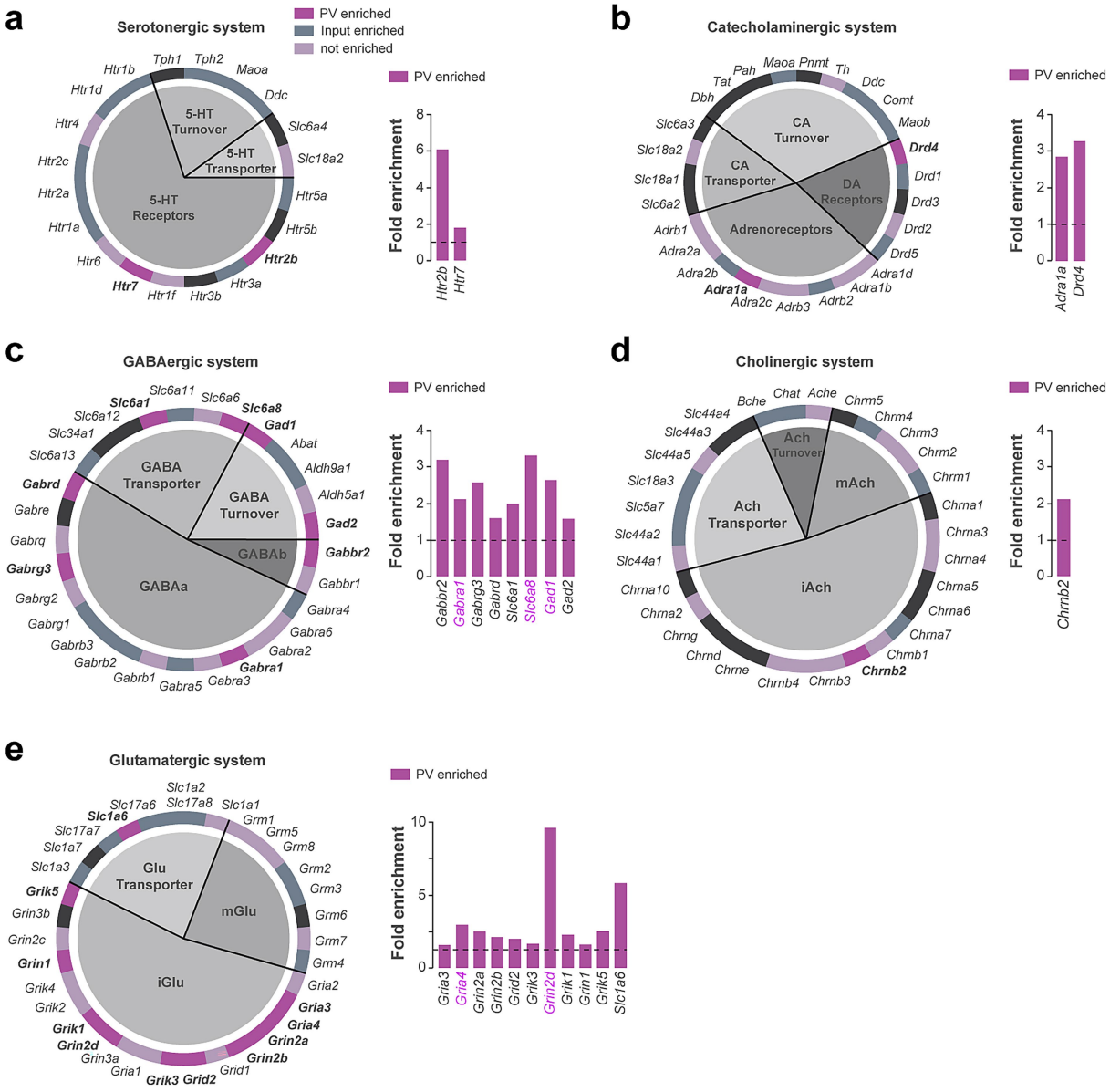

FIGURE 4
Neurotransmitter systems-related genes enriched in DS PV interneurons. Pie chart and fold enrichment graphs of DS PV genes within the **(a)** serotoninergic, **(b)** catecholaminergic, **(c)** GABAergic, **(d)** cholinergic and **(e)** glutamatergic systems. In dark purple are highlighted the genes enriched in the pellet, in gray the ones enriched in the inputs, in light purple the ones detected but not enriched and in black those not found in either the pellet or the input. Enriched genes in common between DS and Acb are highlighted in magenta. Gray horizontal bars above fold enrichment graphs represent subclasses to which the genes belong, shown in the associated pie chart of the system.

interneurons enriched genes among 6 core families of transcription (Supplementary Figure 5). The classification was further refined by analyzing the distribution DS PV neurons enriched genes within each transcription factors subfamilies. The filtering of enriched genes for a FC > 4 allowed the description of a putative transcription factors landscape of DS PV interneurons comprising 5 members of the basic domain groups (*Tfap2b, Hes3, Bach2, Maf, Mafb*) (Supplementary Figure 5a), 1 member of beta scaffold factors (*Lin28b*) (Supplementary Figure 5b), 8 transcripts from the helix-turn helix group (*Onecut2, Satb1, Arid3a, Arx, Barx2, Lhx1, Six4, Pou5f2*) (Supplementary Figure 5c), 4 genes from other alpha helix groups (*Sox12, Sox6, Tox2, Tox3*) (Supplementary Figure 5d), 5 transcripts from the unclassified structure (*Hmga1b, Pura, Prug, Zfp318, Zfp750*) (Supplementary Figure 5e) and 11 members of the zinc coordinating group (*Esrrb, Essrg, Nr6a1, Zfp618, Zim1, Gm14308, Gm14408, Gm14443, Prdm11, Scrt1, Scrt2*) (Supplementary Figure 5f). Among all the genes encoding transcription factors enriched in the DS PV neurons, 75 transcripts were also found in the Acb PV neurons dataset (colored transcripts) with percentages of overlap ranging from 40% for the basic domain groups (8 out of 20 genes in common) and 35% for the helix-turn helix group (20 out of 57 common transcripts) to 12.5% for the beta scaffold factors (1 gene out of 8 genes) (Supplementary Figures 5a–c).

10.3389/fncel.2025.1648461

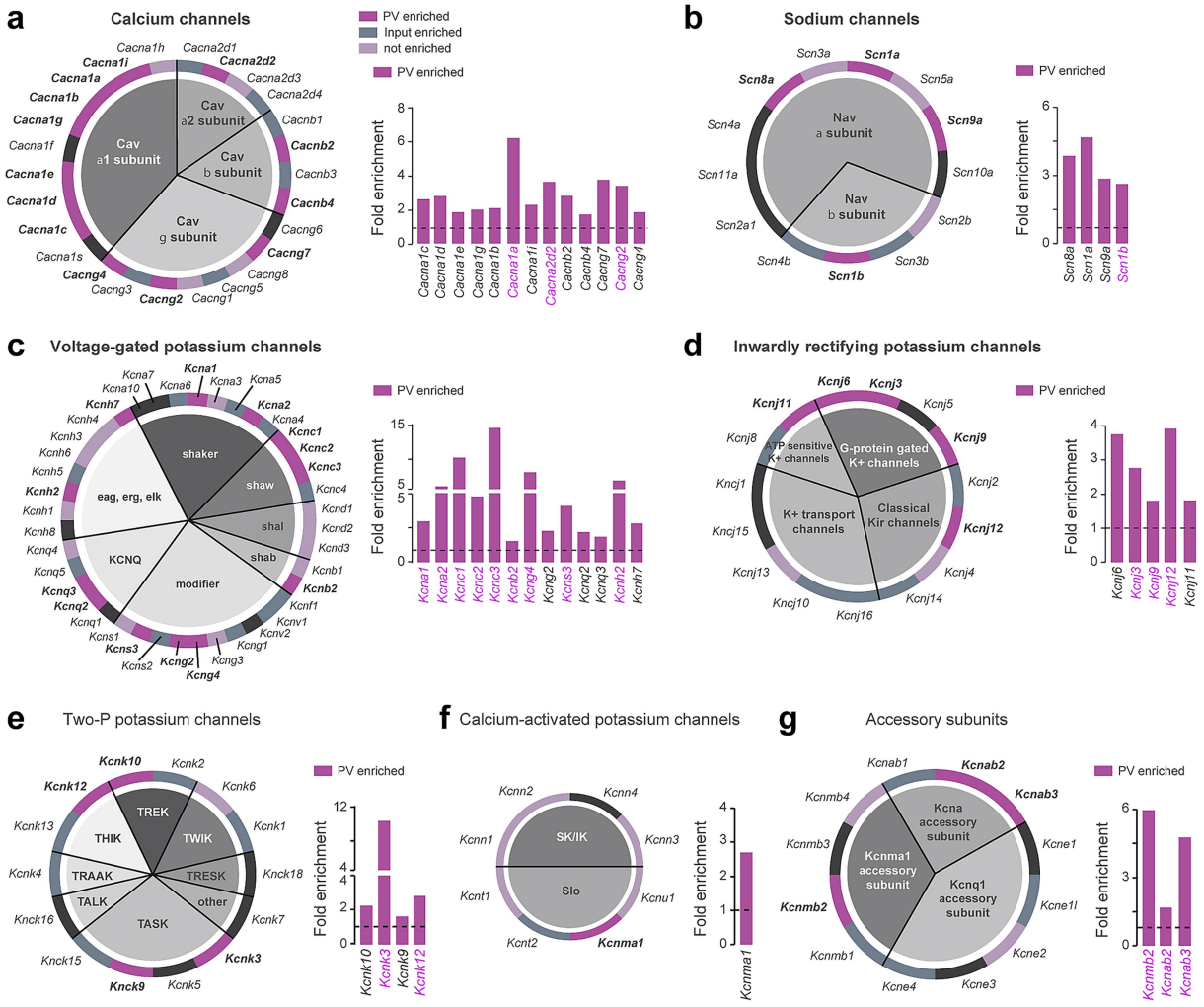

FIGURE 5
Ion channel genes enriched in DS PV interneurons. Pie chart and fold enrichment graphs of DS PV genes encoding for **(a)** calcium channels, **(b)** sodium channels, **(c)** voltage-gated potassium channels, **(d)** inwardly rectifying potassium channels, **(e)** two-P potassium channels, **(f)** calcium-activated potassium channels and **(g)** channels' accessory subunits. In dark purple are highlighted the genes enriched in the pellet, in gray the ones enriched in the inputs, in light purple the ones detected but not enriched and in black those not found in either the pellet or the input. Enriched genes in common between DS and Acb are highlighted in magenta. Gray horizontal bars above fold enrichment graphs represent subclasses to which the genes belong, shown in the associated pie chart of the system.

Translatome of DS PV neurons upon repeated d-amphetamine exposure

Previous works showed that striatal PV interneurons were required for the action of psychostimulant drugs (Wang et al., 2018; Wiltschko et al., 2010). We therefore sought to determine the impact of repeated exposure to d-amphetamine on the DS PV interneurons translatome. *Pvalb-Ribotag* mice used for RNAseq were administered either saline or d-amphetamine (5 mg/kg, i.p.) for 5 consecutive days during which psychomotor responsiveness was measured in a circular corridor (Supplementary Figure 6). As expected, d-amphetamine-treated mice exhibited a robust increase in both horizontal (locomotion) and vertical (rearings) locomotor activity as compared to saline-treated mice (Supplementary Figures 6a,b, $p = 0.003$ (locomotion) and $p = 0.007$ (rearings) at day1, $p < 0.0001$ (locomotion) and $p = 0.0238$ (rearings) at day 5). Although repeated d-amphetamine administration triggered a robust conditioned locomotor response to the context, mice failed to develop locomotor sensitization and strongly decreased their rearing behaviors at the expense of the development of stereotyped behaviors (Supplementary Figures 6b–d). To detect stable modifications, tagged ribosomes-bound mRNAs from DS PV interneurons were isolated 3 days after the last administration of d-amphetamine and compared to DS PV interneurons isolated mRNAs from saline-treated *Pvalb-Ribotag* mice (Supplementary Figure 6e). Comparison between PV neurons saline and d-amphetamine samples identified only one differentially translated transcripts (*Gm20683*) between these groups (Supplementary Figure 6e). In contrast, when input fractions from saline and d-amphetamine samples were compared, we identified 1 downregulated and 96 upregulated transcripts in d-amphetamine

group most of them being microtubule cytoskeleton-related genes (Supplementary Figure 6f).

Translatome of DS PV neurons following standard and high palatable food-seeking behaviors

To evaluate whether reward type and contingency impacted gene expression in DS PV neurons, food-restricted *Pvalb-Ribotag* mice were divided into two groups based on pellet type: a high-palatable diet or a standard chow (Castell et al., 2024). Within each dietary condition, animals were subsequently allocated to two groups: master mice, which earned food rewards through lever pressing, and yoked mice, which passively received a pellet each time their paired master obtained one. During the initial FR1 schedule (days 1 to 5), behavioral performance began to diverge after the third training session (Figure 6a, upper panel). Compared to master mice given regular chow, master mice trained for high-palatable rewards exhibited a significantly higher number of active lever presses ($p < 0.0001$) (Figure 6a, upper panel; Supplementary Table 4). Accordingly, both high-palatable masters and their yoked counterparts received a greater number of pellets than the standard food groups ($p < 0.0001$) (Figure 6a, middle panel and Supplementary Table 4). As expected, lever pressing remained low and stable across days in yoked animals, reflecting the absence of action-outcome contingency (Figure 6a, upper panel; Supplementary Table 4). Upon transition to an FR5 schedule (days 6–9), high-palatable masters showed a progressive increase in lever pressing across sessions. In contrast, standard food masters exhibited a marked increase in responding on the first day of FR5, followed by performance stabilization, as reflected in both lever press frequency and pellet delivery (Figure 6a, upper and middle panels; Supplementary Table 4). From day 10 to 15, animals were returned to *ad libitum* feeding. Under these conditions, both groups of master mice reduced operant responding, consistent with reduced motivational drive as their physiological needs were now met. High-palatable masters continued to lever press at a higher rate than standard chow masters, although both groups demonstrated a progressive decline in responding over time (Figure 6a, upper panel; Supplementary Table 4). To further highlight the behavioral dissociation between master and yoked groups, we quantified food magazine visits (Figure 6a, lower panel; Supplementary Table 4). During the food-restricted phase, yoked mice exhibited a higher frequency of magazine checks compared to their corresponding

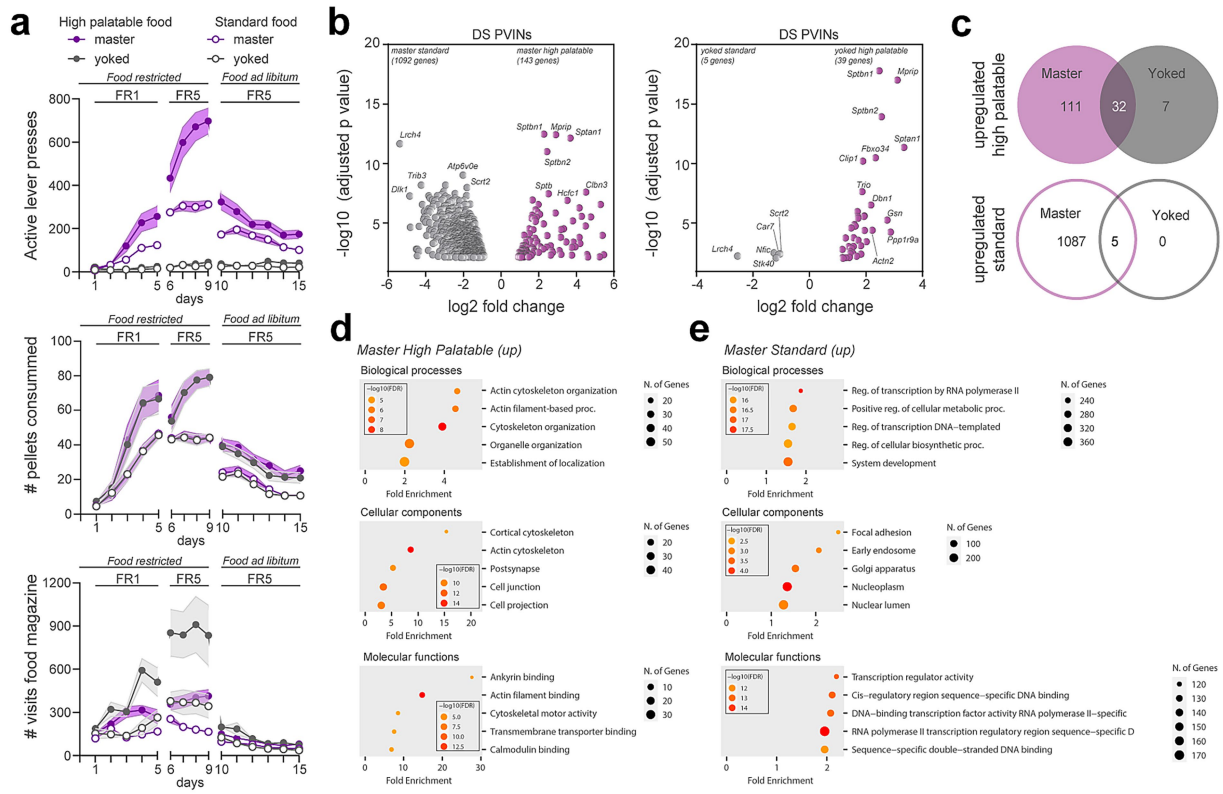

FIGURE 6
Gene expression changes induced in PV interneurons by food-seeking behaviors. **(a)** Operant behavioral task performance in master (purple) and yoked (gray). Number of active lever presses, pellet consumed and visits to the distributor compartment (magazine) are shown for highly palatable (filled symbols) or standard food (empty symbols) during simple (fixed ratio 1, FR1) and more demanding tasks (FR5) in food restricted animals and upon reintroduction of ad libitum food. **(b)** Volcano plots of significantly enriched or de-enriched genes in DS PV interneurons of master (left) and yoked (right) mice 1 day after the last session of food-seeking behavior. **(c)** Venn diagrams showing the number of overlapping upregulated genes in master and yoked mice under highly palatable and standard food diet. **(d,e)** Gene ontology analysis of the biological processes, cellular components and molecular functions of the upregulated genes in master animals under the two food conditions. (Detailed statistical analysis in Supplementary Table 4: 6a-c).

master mice consistent with the non-contingent nature of reward delivery in yoked animals. This pattern was abolished under *ad libitum feeding*, during which all groups displayed comparable low levels of food magazine inspection (Figure 6a, lower panel; Supplementary Table 4).

One day after the last session, immunoprecipitation of tagged ribosomes was performed and isolated DS PV interneurons mRNAs from the 4 groups were analyzed by high-throughput RNAseq. Paired comparisons between master groups (standard vs. high palatable) revealed the highest number of the differentially translated transcripts (Figure 6b; Supplementary Table 2). Indeed, 1,092 genes were found to be enriched in DS PV interneurons in standard food masters whereas 143 genes were more expressed in high palatable food masters (Figure 6b). In contrast, analysis between yoked groups (standard vs. high palatable food) identified 44 genes displaying differential expression DS PV interneurons (Figure 6b). However, these latter changes were unlikely directly linked to food palatability as 37 genes out of 44 were similarly modified between standard and high palatable master mice, suggesting that most of the changes observed in DS PV interneurons were a snapshot of the interaction between food-seeking behavior and the palatability (Figure 6b). Comparison of upregulated genes in master and yoked mice fed a high-palatable diet revealed 32 genes commonly upregulated in both groups, indicating that these genes may be associated with the sucrose content of the diet rather than operant behavioral contingency (Figure 6c). In contrast, only 5 genes were commonly upregulated between master and yoked mice on the standard diet, suggesting a more limited shared transcriptional response under these conditions (Figure 6c). To get insights into the biological functions of the changes observed we conducted GO enrichment analysis. We found that most of the genes upregulated in high palatable food master mice were related to actin cytoskeleton organization (Figure 6d). Although transcripts related to tubulin, actin, cell adhesion and ECM regulation were also increased in standard master mice, GO terms associated to transcription were the most represented in this group (Figures 6d,e) (Gallegos et al., 2023; Manz et al., 2022; Wang et al., 2018). Among the 1,092 upregulated genes, 155 were identified as transcription factors distributed in the 6 core families.

Discussion

The present work provides a comprehensive analysis of translated mRNAs enriched in the PV interneurons of the dorsal striatum. Our approach using *Pvalb-Ribotag* mice allowed the identification of more than 2,700 protein-coding transcripts with a fold-change > 1.5 enriched in DS PV interneurons. Our study extends previous single-cell RNAseq works revealing the molecular heterogeneity of striatal PV interneurons (Gallegos et al., 2023; Muñoz-Manchado et al., 2018; Saunders et al., 2018). Finally, our work also unveiled the potential limitation of using the *Pvalb-IRES-Cre* mouse line for studies aiming to investigate the role of PV interneurons across both the dorsal and ventral striatum.

Since the early 2000s, the *Pvalb-IRES-Cre* mouse line has been extensively used to study the role and function of striatal PV interneurons. In most cases, this has been achieved by transducing engineered viral vectors selectively in PV interneurons allowing to establish a causal link between their activity and diverse striatal-dependent behaviors including choice execution (Gage et al., 2010), learning strategies (Owen et al., 2018), habits formation (O'Hare et al., 2017) as well as early phase of reward conditioning (Lee et al., 2018). We therefore decided to use the *Pvalb-IRES-Cre* mouse line to generate *Pvalb-Ribotag* mice with the aim to perform the in-depth analysis of the translatome of striatal PV interneurons. However, during the characterization of this mouse line, we were surprised by the unexpectedly low rate of recombination. Indeed, despite the fact that the *Pvalb-IRES-Cre* mouse line is a knockin to the endogenous *Pvalb* promoter/enhancer elements (Hippenmeyer et al., 2005), we were unable to detect any labeling in the ventral striatum. In the DS the expression of HA was restricted to ~60% of endogenous PV interneurons with a higher level of recombination in the DLS compared to the DMS reminiscent to the medio-lateral gradient of DS PV interneurons (Berke et al., 2004; Fino et al., 2018). Because the ability of the Cre line to recombine the reporter transgene depends on the nature of that transgene, we initially thought that low recombination efficiency was due to the Ribotag allele not being inserted in the ROSA locus (Sanz et al., 2009). However, we rapidly ruled out this hypothesis as we found a similar rate of recombination with two reporter mouse lines carrying the tdTomato (Ai14) or the channelrhodopsin (Ai32) both inserted in the ROSA locus (Madisen et al., 2012, 2010). An alternative hypothesis would be that in the subset of striatal interneurons expressing low levels of PV, the threshold of Cre expression required to recombine the transgenes is not met, thereby resulting in a large proportion of PV interneurons remaining unlabeled (Liu et al., 2013). Our results extend previous observations of a similarly low rate of recombination in the perirhinal cortex (Nigro et al., 2021) and cerebellum (Wang et al., 2022). Future studies using the newly developed AAV toolbox enabling to target striatal PV interneurons with high precision should overcome this limitation (Hunker et al., 2025).

Despite this limitation, we successfully trapped HA-tagged cells allowing us to establish the translatome of this restricted population of DS PV interneurons. Comparison of our results with previous datasets suggested that our translatome most likely overlap with the *Pvalb-Pthlh* sub population (Muñoz-Manchado et al., 2018). Moreover, our cross-analysis with the translatome of the Acb identified 1,015 transcripts enriched in striatal PV interneurons irrespective of their location (Gallegos et al., 2023). This number, representing about 30% of the PV-enriched genes in both DS and Acb suggests that PV interneurons display a high level of molecular heterogeneity throughout the dorso-ventral axis of the striatum, an observation reminiscent to the one previously reported for the translatomes of *Drd1-and Drd2*-SPNs (Montalban et al., 2022; Puighermanal et al., 2020). It will be interesting to determine in the future to what extent the differences observed between the Acb and DS PV interneuron translatomes are functionally relevant and potentially related to the distinct developmental origins of PV interneurons (Knowles et al., 2021).

The use of several databases allowed us to refine our analysis based on systematic functional gene classifications. For instance, the identification of a unique ECM and adhesion molecule signature for DS PV interneurons provides a strong molecular rationale for the presence of perineuronal nets enwrapping PV interneurons (Santos-Silva et al., 2024). Moreover, our system-based classification afforded important insights regarding their electrophysiological signatures. Thus, our analysis revealed the enrichment genes encoding various classes of ion channels previously identified to (i) facilitate their rapid

repolarization and sustained fast-spiking activity (*Kcna1, Kcna2, Kcnc1,* and *Kcnc2*) (Hu et al., 2014), (ii) maintain their resting membrane potential and regulate their excitability (*Kcnj3, Kcnj6, Kcnj11*, and *Kcnj12*) (Du et al., 1996; Furdan et al., 2025; Muñoz-Manchado et al., 2018). Interestingly, the transcripts that support these electrophysiological features are enriched in both DS and Acb PV interneurons, representing a genetic portfolio linked to the function rather than the location of these cells. DS PV interneurons also exhibited marked upregulation of several transcripts encoding calcium (*Cacna1a*, *Cacng7*, *Cacng2, Cacna2d2*) and sodium (*Scn1a*, *Scn8a*, *Scn9a, Scn1b*) channels underlying their electrophysiological properties (Ferguson et al., 2023; Lupien-Meilleur et al., 2021; Rendón-Ochoa et al., 2018). However, it is important to keep in mind that our dataset most likely reflects the translatome of PV interneurons located in DLS and that probably a different, but partly overlapping, set of ion channels may explain some of the electrophysiological features of DMS PV interneurons (Koós and Tepper, 1999; Monteiro et al., 2018). We also identified enriched transcripts that have been previously associated with important functions of PV interneurons in other brain areas. For instance, DS PV interneurons are enriched in *Drd4* and *Errb4* transcripts which encode the dopamine D4 receptor and the neuregulin receptor respectively, providing a potential mechanism through which dopamine could modulate gamma oscillations as previously shown in the hippocampus (Andersson et al., 2012). Finally, this dataset classification also represents a valuable resource to interrogate whether pathological conditions associated to gene-related disorders could be ascribed to a dysfunction of PV interneurons. Thus, motor symptoms associated to *GRIN2D-and SLC6A1*-related disorders including dystonia, chorea and hyperactivity and tremor among others (Cha et al., 2025; Chiu et al., 2005; Gawande et al., 2023; Goodspeed et al., 2020, 1993; Vinnakota et al., 2023), could result from dysfunction of these genes encoding the glutamate ionotropic receptor NMDA subunit 2D (*Grin2d*) and the GABA transporter (*Slc6a1*) respectively, which are both highly enriched in DS PV interneurons. In the same line, motor stereotypies associated to the invalidation of the PV enriched gene *Cntnap2* have been causally linked to hyperexcitability of striatal PV interneurons (Thabault et al., 2024). Finally, mice lacking the creatine transporter *Slc6a8* (3-fold enriched in our dataset) selectively in PV interneurons recapitulated numerous features of the Creatine Transporter Deficiency (CTD), an X-linked neurometabolic disorder presenting with intellectual disability, autistic-like features, and epilepsy (Ghirardini et al., 2023). Future studies can use the same strategy to determine whether other PV-enriched genes identified in our dataset are critical for the normal function of DS PV interneurons and if their deregulation is central in disease pathogenesis.

Previous work indicate that striatal PV interneurons are required for d-amphetamine effects. Thus, DS PV interneurons increased their firing rate in response to a single d-amphetamine administration, an electrophysiological response positively correlated with increased locomotion (Wiltschko et al., 2010). The silencing of Acb PV interneurons impaired d-amphetamine-induced psychomotor sensitization and conditioned place preference (Wang et al., 2018). Finally, important transcriptional regulations have been identified in Acb PV interneurons in response to acute and repeated d-amphetamine exposure (Gallegos et al., 2023). Surprisingly, our analysis identified only 1 transcript (*Gm20683*) differentially regulated in DS PV interneurons of mice repeatedly administered with d-amphetamine compared to saline-treated mice. Apart from the regions analyzed (DS vs. Acb), other factors including the experimental design could account for these differences. Indeed, Gallegos and colleagues injected d-amphetamine at a dose of 3 mg/kg for 7 days, while in our case mice were administered with 5 mg/kg of d-amphetamine once daily during 5 days. Moreover, the different delay between the last administration of d-amphetamine and the extraction of samples (24 h against 3 days in our protocol) might also explain the lack of differentially regulated genes in our RNAseq.

Besides this, we identified long-lasting changes in the translatome of DS PV interneurons in mice trained to obtain standard or high palatable food pellets compared to yoked-groups receiving them passively. These results suggest that alterations in gene expression in DS PV interneurons may occur under specific conditions, notably during behavioral paradigms requiring optimized execution of sequential motor plans, such as the FR5 reinforcement schedule, in which mice pressed the lever more than 700 times on average to obtain highly palatable rewards. Interestingly, among the upregulated genes, several encode for cell adhesion molecules and cytoskeleton proteins necessary for the function of PV interneurons synapses. Thus, remodeling of DS PV interneurons translatome could contribute to the plasticity underlying the rearrangement of striatal network activity required to optimize motor plans.

Overall, our findings provide a comprehensive molecular resource to study dorsal striatal PV interneurons and highlight their dynamic translatome as a potential substrate for experience-dependent plasticity relevant to both motor function and neuropsychiatric disorders.

Data availability statement

Sequence data have been deposited in Gene Expression Omnibus, accession codes GSE308752 and GSE308753. The data supporting the findings of this study are available within the paper and its Supplementary materials files or available from the corresponding author upon reasonable request.

Ethics statement

All animal procedures were conducted in accordance with the guidelines of the French Agriculture and Forestry Ministry for handling animals (authorization number/license B34-172-41) and approved by the relevant local and national ethics committees (authorization APAFIS#38912). The study was conducted in accordance with the local legislation and institutional requirements.

Author contributions

CN: Data curation, Writing – review & editing, Methodology, Writing – original draft, Formal analysis. LCa: Writing – original draft, Formal analysis, Data curation, Writing – review & editing. ST: Formal analysis, Writing – review & editing, Data curation. MM: Data curation, Methodology, Formal analysis, Writing – review & editing. SR: Visualization, Formal analysis, Writing – review & editing, Methodology. EG: Formal analysis, Data curation, Writing – review

& editing. EC: Validation, Writing – review & editing, Formal analysis. AR: Formal analysis, Data curation, Writing – review & editing. MG: Methodology, Formal analysis, Writing – review & editing. AE-C: Writing – review & editing, Formal analysis, Methodology, Data curation. AQ: Resources, Writing – review & editing, Methodology. FB: Writing – original draft, Writing – review & editing, Investigation, Formal analysis, Visualization, Methodology. EV: Writing – original draft, Funding acquisition, Data curation, Writing – review & editing, Conceptualization, Supervision. LCu: Writing – original draft, Formal analysis, Conceptualization, Funding acquisition, Supervision, Methodology, Writing – review & editing, Data curation, Investigation.

Funding

The author(s) declare that financial support was received for the research and/or publication of this article. This work was supported by CNRS, INSERM, Fondation pour la Recherche Médicale (EQU202203014705, EV), the French National Research Agency (ANR-20-CE14-0020, ANR-21-CE16-0028, ANR-16-CE16-0018 to EV). LCu was supported by MINECO (Ramon y Cajal) fellowship (Spain) (RYC2022-037332-I), H2020-MSCA-IF-2020 (Proposal 101028078; MITORett) and the postdoctoral Labex EpiGenMed fellowship (Investissements d'avenir, ANR-10-LABX-12-01). CNAG acknowledges the support of the Spanish Ministry of Science and Innovation through the Instituto de Salud Carlos III and the 2014–2020 Smart Growth Operating Program, co-financed with the European Regional Development Fund (MINECO/FEDER, BIO2015-71792-P). We also acknowledge the support of the Generalitat de Catalunya through the Departament de Salut, the Departament de Recerca i Universitats and the Departament d'Empresa i Coneixement.

Acknowledgments

The authors thank all the lab members and the Microscopy Imaging Platform from IGF and INM (Biocampus). The authors also thank iExplore at IGF for their involvement in the maintenance and breeding of the colonies. The authors thank Anne E. West for her insightful comments regarding the variability of recombination in the striatum using *Pval-IRES-Cre* line in combination with the different mouse reporter lines.

Conflict of interest

The authors declare that the research was conducted in the absence of any commercial or financial relationships that could be construed as a potential conflict of interest.

The author(s) declared that they were an editorial board member of Frontiers, at the time of submission. This had no impact on the peer review process and the final decision.

Generative AI statement

The authors declare that no Gen AI was used in the creation of this manuscript.

Any alternative text (alt text) provided alongside figures in this article has been generated by Frontiers with the support of artificial intelligence and reasonable efforts have been made to ensure accuracy, including review by the authors wherever possible. If you identify any issues, please contact us.

Publisher's note

Supplementary material

The Supplementary material for this article can be found online at: https://www.frontiersin.org/articles/10.3389/fncel.2025.1648461/full#supplementary-material

References

Andersson, R. H., Johnston, A., Herman, P. A., Winzer-Serhan, U. H., Karavanova, I., Vullhorst, D., et al. (2012). Neuregulin and dopamine modulation of hippocampal gamma oscillations is dependent on dopamine D4 receptors. *Proc. Natl. Acad. Sci. USA* 109, 13118–13123. doi: 10.1073/pnas.1201011109

Arias-García, M. A., Tapia, D., Laville, J. A., Calderón, V. M., Ramiro-Cortés, Y., Bargas, J., et al. (2018). Functional comparison of corticostriatal and thalamostriatal postsynaptic responses in striatal neurons of the mouse. *Brain Struct. Funct.* 223, 1229–1253. doi: 10.1007/s00429-017-1536-6

Berke, J. D., Okatan, M., Skurski, J., and Eichenbaum, H. B. (2004). Oscillatory entrainment of striatal neurons in freely moving rats. *Neuron* 43, 883–896. doi: 10.1016/j.neuron.2004.08.035

Burguière, E., Monteiro, P., Feng, G., and Graybiel, A. M. (2013). Optogenetic stimulation of lateral orbitofronto-striatal pathway suppresses compulsive behaviors. *Science* 340, 1243–1246. doi: 10.1126/science.1232380

Castell, L., Le Gall, V., Cutando, L., Petit, C. P., Puighermanal, E., Makrini-Maleville, L., et al. (2024). Dopamine D2 receptors in WFS1-neurons regulate food-seeking and avoidance behaviors. *Prog. Neuro-Psychopharmacol. Biol. Psychiatry* 129:110883. doi: 10.1016/j.pnpbp.2023.110883

Cha, J. H., Kim, J. M., Yun, H.-J., Chin, H., Kim, H. J., Kim, W., et al. (2025). Exploring gene-phenotype relationships in GRIN-related neurodevelopmental disorders. *NPJ Genom. Med.* 10:40. doi: 10.1038/s41525-025-00499-z

Chiu, C.-S., Brickley, S., Jensen, K., Southwell, A., Mckinney, S., Cull-Candy, S., et al. (2005). GABA transporter deficiency causes tremor, ataxia, nervousness, and increased GABA-induced tonic conductance in cerebellum. *J. Neurosci.* 25, 3234–3245. doi: 10.1523/JNEUROSCI.3364-04.2005

Choi, K., Holly, E. N., Davatolhagh, M. F., Beier, K. T., and Fuccillo, M. V. (2019). Integrated anatomical and physiological mapping of striatal afferent projections. *Eur. J. Neurosci.* 49, 623–636. doi: 10.1111/ejn.13829

Christensen, A. C., Lensjø, K. K., Lepperød, M. E., Dragly, S.-A., Sutterud, H., Blackstad, J. S., et al. (2021). Perineuronal nets stabilize the grid cell network. *Nat. Commun.* 12:253. doi: 10.1038/s41467-020-20241-w

Cutando, L., Puighermanal, E., Castell, L., Tarot, P., Belle, M., Bertaso, F., et al. (2022). Cerebellar dopamine D2 receptors regulate social behaviors. *Nat. Neurosci.* 25, 900–911. doi: 10.1038/s41593-022-01092-8

Cutando, L., Puighermanal, E., Castell, L., Tarot, P., Bertaso, F., Bonnavion, P., et al. (2021). Regulation of GluA1 phosphorylation by d-amphetamine

and methylphenidate in the cerebellum. *Addict. Biol.* 26:e12995. doi: 10.1111/adb.12995

Dobin, A., Davis, C. A., Schlesinger, F., Drenkow, J., Zaleski, C., Jha, S., et al. (2013). STAR: ultrafast universal RNA-seq aligner. *Bioinformatics* 29, 15–21. doi: 10.1093/bioinformatics/bts635

Du, J., Zhang, L., Weiser, M., Rudy, B., and McBain, C. J. (1996). Developmental expression and functional characterization of the potassium-channel subunit Kv3.1b in parvalbumin-containing interneurons of the rat hippocampus. *J. Neurosci.* 16, 506–518. doi: 10.1523/JNEUROSCI.16-02-00506.1996

Duhne, M., Lara-González, E., Laville, A., Padilla-Orozco, M., Ávila-Cascajares, F., Arias-García, M., et al. (2021). Activation of parvalbumin-expressing neurons reconfigures neuronal ensembles in murine striatal microcircuits. *Eur. J. Neurosci.* 53, 2149–2164. doi: 10.1111/ejn.14670

Ferguson, B., Glick, C., and Huguenard, J. R. (2023). Prefrontal PV interneurons facilitate attention and are linked to attentional dysfunction in a mouse model of absence epilepsy. *eLife* 12:e78349. doi: 10.7554/eLife.78349

Fino, E., Vandecasteele, M., Perez, S., Saudou, F., and Venance, L. (2018). Region-specific and state-dependent action of striatal GABAergic interneurons. *Nat. Commun.* 9:3339. doi: 10.1038/s41467-018-05847-5

Furdan, S., Douida, A., Bakos, E., Tiszlavicz, Á., Molnár, G., and Tamás, G., (2025). Regulation of input excitability in human and mouse parvalbumin interneurons by Kir potassium channels. bioRxiv [Preprint].

Gage, G. J., Stoetzner, C. R., Wiltschko, A. B., and Berke, J. D. (2010). Selective activation of striatal fast-spiking interneurons during choice execution. *Neuron* 67, 466–479. doi: 10.1016/j.neuron.2010.06.034

Gallegos, D. A., Minto, M., Liu, F., Hazlett, M. F., Aryana Yousefzadeh, S., Bartelt, L. C., et al. (2023). Cell-type specific transcriptional adaptations of nucleus accumbens interneurons to amphetamine. *Mol. Psychiatry* 28, 3414–3428. doi: 10.1038/s41380-022-01466-1

Gawande, D. Y., Narasimhan, S., Shelkar, G. P., Pavuluri, R., Stessman, H. A. F., and Dravid, S. M. (2023). GluN2D subunit in Parvalbumin interneurons regulates prefrontal cortex feedforward inhibitory circuit and molecular networks relevant to schizophrenia. *Biol. Psychiatry* 94, 297–309. doi: 10.1016/j.biopsych.2023.03.020

Ge, S. X., Jung, D., and Yao, R. (2020). ShinyGO: a graphical gene-set enrichment tool for animals and plants. *Bioinformatics* 36, 2628–2629. doi: 10.1093/bioinformatics/btz931

Gerfen, C. R., Paletzki, R., and Heintz, N. (2013). GENSAT BAC cre-recombinase driver lines to study the functional organization of cerebral cortical and basal ganglia circuits. *Neuron* 80, 1368–1383. doi: 10.1016/j.neuron.2013.10.016

Ghirardini, E., Sagona, G., Marquez-Galera, A., Calugi, F., Navarron, C. M., Cacciante, F., et al. (2023). Cell-specific vulnerability to metabolic failure: the crucial role of parvalbumin expressing neurons in creatine transporter deficiency. *Acta Neuropathol. Commun.* 11:34. doi: 10.1186/s40478-023-01533-w

Gittis, A. H., Leventhal, D. K., Fensterheim, B. A., Pettibone, J. R., Berke, J. D., and Kreitzer, A. C. (2011). Selective inhibition of striatal fast-spiking interneurons causes dyskinesias. *J. Neurosci.* 31, 15727–15731. doi: 10.1523/JNEUROSCI.3875-11.2011

Gittis, A. H., Nelson, A. B., Thwin, M. T., Palop, J. J., and Kreitzer, A. C. (2010). Distinct roles of GABAergic interneurons in the regulation of striatal output pathways. *J. Neurosci.* 30, 2223–2234. doi: 10.1523/JNEUROSCI.4870-09.2010

Gokce, O., Stanley, G. M., Treutlein, B., Neff, N. F., Camp, J. G., Malenka, R. C., et al. (2016). Cellular taxonomy of the mouse striatum as revealed by single-cell RNA-Seq. *Cell Rep.* 16, 1126–1137. doi: 10.1016/j.celrep.2016.06.059

Goodspeed, K., Demarest, S., Johannesen, K., Kang, J., Lal, D., and Angione, K. (1993). "SLC6A1-related neurodevelopmental disorder" in GeneReviews®. eds. M. P. Adam, J. Feldman, G. M. Mirzaa, R. A. Pagon, S. E. Wallace and A. Amemiya (Seattle, Seattle (WA): University of Washington).

Goodspeed, K., Pérez-Palma, E., Iqbal, S., Cooper, D., Scimemi, A., Johannesen, K. M., et al. (2020). Current knowledge of SLC6A1-related neurodevelopmental disorders. *Brain Commun* 2:fcaa170. doi: 10.1093/braincomms/fcaa170

Graveland, G. A., and DiFiglia, M. (1985). The frequency and distribution of medium-sized neurons with indented nuclei in the primate and rodent neostriatum. *Brain Res.* 327, 307–311. doi: 10.1016/0006-8993(85)91524-0

Graybiel, A. M., and Grafton, S. T. (2015). The striatum: where skills and habits meet. *Cold Spring Harb. Perspect. Biol.* 7:a021691. doi: 10.1101/cshperspect.a021691

Härtig, W., Meinicke, A., Michalski, D., Schob, S., and Jäger, C. (2022). Update on Perineuronal net staining with *Wisteria floribunda* agglutinin (WFA). *Front. Integr. Neurosci.* 16:851988. doi: 10.3389/fnint.2022.851988

Hazlett, M. F., Hall, V. L., Patel, E., Halvorsen, A., Calakos, N., and West, A. E. (2024). The Perineuronal net protein Brevican acts in nucleus Accumbens Parvalbumin-expressing interneurons of adult mice to regulate excitatory synaptic inputs and motivated Behaviors. *Biol. Psychiatry* 96, 694–707. doi: 10.1016/j.biopsych.2024.02.003

Hintiryan, H., Foster, N. N., Bowman, I., Bay, M., Song, M. Y., Gou, L., et al. (2016). The mouse cortico-striatal projectome. *Nat. Neurosci.* 19, 1100–1114. doi: 10.1038/nn.4332

Hippenmeyer, S., Vrieseling, E., Sigrist, M., Portmann, T., Laengle, C., Ladle, D. R., et al. (2005). A developmental switch in the response of DRG neurons to ETS transcription factor signaling. *PLoS Biol.* 3:e159. doi: 10.1371/journal.pbio.0030159

Hu, H., Gan, J., and Jonas, P. (2014). Interneurons. Fast-spiking, parvalbumin$^+$ GABAergic interneurons: from cellular design to microcircuit function. *Science* 345:1255263. doi: 10.1126/science.1255263

Hunker, A. C., Wirthlin, M. E., Gill, G., Johansen, N. J., Hooper, M., Omstead, V., et al. (2025). Enhancer AAV toolbox for accessing and perturbing striatal cell types and circuits. *Neuron* 113, 1507–1524.e17. doi: 10.1016/j.neuron.2025.04.035

Hunnicutt, B. J., Jongbloets, B. C., Birdsong, W. T., Gertz, K. J., Zhong, H., and Mao, T. (2016). A comprehensive excitatory input map of the striatum reveals novel functional organization. *eLife* 5:e19103. doi: 10.7554/eLife.19103

Knowles, R., Dehorter, N., and Ellender, T. (2021). From progenitors to progeny: shaping striatal circuit development and function. *J. Neurosci.* 41, 9483–9502. doi: 10.1523/JNEUROSCI.0620-21.2021

Kolberg, L., Raudvere, U., Kuzmin, I., Adler, P., Vilo, J., and Peterson, H. (2023). G:profiler-interoperable web service for functional enrichment analysis and gene identifier mapping (2023 update). *Nucleic Acids Res.* 51, W207–W212. doi: 10.1093/nar/gkad347

Koós, T., and Tepper, J. M. (1999). Inhibitory control of neostriatal projection neurons by GABAergic interneurons. *Nat. Neurosci.* 2, 467–472. doi: 10.1038/8138

Kreitzer, A. C. (2009). Physiology and pharmacology of striatal neurons. *Annu. Rev. Neurosci.* 32, 127–147. doi: 10.1146/annurev.neuro.051508.135422

Kreitzer, A. C., and Malenka, R. C. (2008). Striatal plasticity and basal ganglia circuit function. *Neuron* 60, 543–554. doi: 10.1016/j.neuron.2008.11.005

Law, C. W., Chen, Y., Shi, W., and Smyth, G. K. (2014). Voom: precision weights unlock linear model analysis tools for RNA-seq read counts. *Genome Biol.* 15:R29. doi: 10.1186/gb-2014-15-2-r29

Lee, K., Holley, S. M., Shobe, J. L., Chong, N. C., Cepeda, C., Levine, M. S., et al. (2018). Parvalbumin interneurons modulate striatal output and enhance performance during associative learning. *Neuron* 99:239. doi: 10.1016/j.neuron.2018.06.034

Li, B., and Dewey, C. N. (2011). RSEM: accurate transcript quantification from RNA-Seq data with or without a reference genome. *BMC Bioinformatics* 12:323. doi: 10.1186/1471-2105-12-323

Liu, J., Willet, S. G., Bankaitis, E. D., Xu, Y., Wright, C. V. E., and Gu, G. (2013). Non-parallel recombination limits Cre-LoxP-based reporters as precise indicators of conditional genetic manipulation. *Genesis* 51, 436–442. doi: 10.1002/dvg.22384

Lupien-Meilleur, A., Jiang, X., Lachance, M., Taschereau-Dumouchel, V., Gagnon, L., Vanasse, C., et al. (2021). Reversing frontal disinhibition rescues behavioural deficits in models of CACNA1A-associated neurodevelopment disorders. *Mol. Psychiatry* 26, 7225–7246. doi: 10.1038/s41380-021-01175-1

Madisen, L., Mao, T., Koch, H., Zhuo, J., Berenyi, A., Fujisawa, S., et al. (2012). A toolbox of Cre-dependent optogenetic transgenic mice for light-induced activation and silencing. *Nat. Neurosci.* 15, 793–802. doi: 10.1038/nn.3078

Madisen, L., Zwingman, T. A., Sunkin, S. M., Oh, S. W., Zariwala, H. A., Gu, H., et al. (2010). A robust and high-throughput Cre reporting and characterization system for the whole mouse brain. *Nat. Neurosci.* 13, 133–140. doi: 10.1038/nn.2467

Mallet, N., Le Moine, C., Charpier, S., and Gonon, F. (2005). Feedforward inhibition of projection neurons by fast-spiking GABA interneurons in the rat striatum in vivo. *J. Neurosci.* 25, 3857–3869. doi: 10.1523/JNEUROSCI.5027-04.2005

Manz, K. M., Coleman, B. C., Jameson, A. N., Ghose, D. G., Patel, S., and Grueter, B. A. (2022). Cocaine restricts nucleus accumbens feedforward drive through a monoamine-independent mechanism. *Neuropsychopharmacology* 47, 652–663. doi: 10.1038/s41386-021-01167-3

Marsden, C. D., and Obeso, J. A. (1994). The functions of the basal ganglia and the paradox of stereotaxic surgery in Parkinson's disease. *Brain* 117, 877–897. doi: 10.1093/brain/117.4.877

Märtin, A., Calvigioni, D., Tzortzi, O., Fuzik, J., Wärnberg, E., and Meletis, K. (2019). A Spatiomolecular map of the striatum. *Cell Rep.* 29, 4320–4333.e5. doi: 10.1016/j.celrep.2019.11.096

Mondragón-González, S. L., Schreiweis, C., and Burguière, E. (2024). Closed-loop recruitment of striatal interneurons prevents compulsive-like grooming behaviors. *Nat. Neurosci.* 27, 1148–1156. doi: 10.1038/s41593-024-01633-3

Montalban, E., Giralt, A., Taing, L., Schut, E. H. S., Supiot, L. F., Castell, L., et al. (2022). Translational profiling of mouse dopaminoceptive neurons reveals region-specific gene expression, exon usage, and striatal prostaglandin E2 modulatory effects. *Mol. Psychiatry* 27, 2068–2079. doi: 10.1038/s41380-022-01439-4

Monteiro, P., Barak, B., Zhou, Y., McRae, R., Rodrigues, D., Wickersham, I. R., et al. (2018). Dichotomous parvalbumin interneuron populations in dorsolateral and dorsomedial striatum. *J. Physiol.* 596, 3695–3707. doi: 10.1113/JP275936

Muñoz-Manchado, A. B., Bengtsson Gonzales, C., Zeisel, A., Munguba, H., Bekkouche, B., Skene, N. G., et al. (2018). Diversity of interneurons in the dorsal striatum revealed by single-cell RNA sequencing and PatchSeq. *Cell Rep.* 24, 2179–2190.e7. doi: 10.1016/j.celrep.2018.07.053

Nigro, M. J., Kirikae, H., Kjelsberg, K., Nair, R. R., and Witter, M. P. (2021). Not all that is gold glitters: PV-IRES-Cre mouse line shows low efficiency of Labeling of Parvalbumin interneurons in the Perirhinal cortex. *Front Neural Circuits* 15:781928. doi: 10.3389/fncir.2021.781928

O'Hare, J. K., Li, H., Kim, N., Gaidis, E., Ade, K., Beck, J., et al. (2017). Striatal fast-spiking interneurons selectively modulate circuit output and are required for habitual behavior. *eLife* 6:e26231. doi: 10.7554/eLife.26231

Oh, S. W., Harris, J. A., Ng, L., Winslow, B., Cain, N., Mihalas, S., et al. (2014). A mesoscale connectome of the mouse brain. *Nature* 508, 207–214. doi: 10.1038/nature13186

Owen, S. F., Berke, J. D., and Kreitzer, A. C. (2018). Fast-spiking interneurons supply feedforward control of bursting, calcium, and plasticity for efficient learning. *Cell* 172, 683–695.e15. doi: 10.1016/j.cell.2018.01.005

Pan, W. X., Mao, T., and Dudman, J. T. (2010). Inputs to the dorsal striatum of the mouse reflect the parallel circuit architecture of the forebrain. *Front. Neuroanat.* 4:147. doi: 10.3389/fnana.2010.00147

Picelli, S., Faridani, O. R., Björklund, A. K., Winberg, G., Sagasser, S., and Sandberg, R. (2014). Full-length RNA-seq from single cells using Smart-seq2. *Nat. Protoc.* 9, 171–181. doi: 10.1038/nprot.2014.006

Planert, H., Berger, T. K., and Silberberg, G. (2013). Membrane properties of striatal direct and indirect pathway neurons in mouse and rat slices and their modulation by dopamine. *PLoS One* 8:e57054. doi: 10.1371/journal.pone.0057054

Puighermanal, E., Castell, L., Esteve-Codina, A., Melser, S., Kaganovsky, K., Zussy, C., et al. (2020). Functional and molecular heterogeneity of D2R neurons along dorsal ventral axis in the striatum. *Nat. Commun.* 11:1957. doi: 10.1038/s41467-020-15716-9

Rendón-Ochoa, E. A., Hernández-Flores, T., Avilés-Rosas, V. H., Cáceres-Chávez, V. A., Duhne, M., Laville, A., et al. (2018). Calcium currents in striatal fast-spiking interneurons: dopaminergic modulation of CaV1 channels. *BMC Neurosci.* 19:42. doi: 10.1186/s12868-018-0441-0

Ritchie, M. E., Phipson, B., Wu, D., Hu, Y., Law, C. W., Shi, W., et al. (2015). Limma powers differential expression analyses for RNA-sequencing and microarray studies. *Nucleic Acids Res.* 43:e47. doi: 10.1093/nar/gkv007

Roberts, B. M., White, M. G., Patton, M. H., Chen, R., and Mathur, B. N. (2019). Ensemble encoding of action speed by striatal fast-spiking interneurons. *Brain Struct. Funct.* 224, 2567–2576. doi: 10.1007/s00429-019-01908-7

Santos-Silva, T., Colodete, D. A. E., Lisboa, J. R. F., Silva Freitas, Í., Lopes, C. F. B., Hadera, V., et al. (2024). Perineuronal nets as regulators of parvalbumin interneuron function: factors implicated in their formation and degradation. *Basic Clin. Pharmacol. Toxicol.* 134, 614–628. doi: 10.1111/bcpt.13994

Sanz, E., Yang, L., Su, T., Morris, D. R., McKnight, G. S., and Amieux, P. S. (2009). Cell-type-specific isolation of ribosome-associated mRNA from complex tissues. *Proc. Natl. Acad. Sci. USA* 106, 13939–13944. doi: 10.1073/pnas.0907143106

Saunders, A., Macosko, E. Z., Wysoker, A., Goldman, M., Krienen, F. M., de Rivera, H., et al. (2018). Molecular diversity and specializations among the cells of the adult mouse brain. *Cell* 174, 1015–1030.e16. doi: 10.1016/j.cell.2018.07.028

Sciamanna, G., Ponterio, G., Mandolesi, G., Bonsi, P., and Pisani, A. (2015). Optogenetic stimulation reveals distinct modulatory properties of thalamostriatal vs corticostriatal glutamatergic inputs to fast-spiking interneurons. *Sci. Rep.* 5:16742. doi: 10.1038/srep16742

Shen, W.-K., Chen, S.-Y., Gan, Z.-Q., Zhang, Y.-Z., Yue, T., Chen, M.-M., et al. (2023). AnimalTFDB 4.0: a comprehensive animal transcription factor database updated with variation and expression annotations. *Nucleic Acids Res.* 51, D39–D45. doi: 10.1093/nar/gkac907

Smith, A. D., and Bolam, J. P. (1990). The neural network of the basal ganglia as revealed by the study of synaptic connections of identified neurones. *Trends Neurosci.* 13, 259–265. doi: 10.1016/0166-2236(90)90106-k

Tepper, J. M., and Bolam, J. P. (2004). Functional diversity and specificity of neostriatal interneurons. *Curr. Opin. Neurobiol.* 14, 685–692. doi: 10.1016/j.conb.2004.10.003

Tepper, J. M., Koós, T., Ibanez-Sandoval, O., Tecuapetla, F., Faust, T. W., and Assous, M. (2018). Heterogeneity and diversity of striatal GABAergic interneurons: update 2018. *Front. Neuroanat.* 12:91. doi: 10.3389/fnana.2018.00091

Thabault, M., Fernandes-Gomes, C., Huot, A.-L., Francheteau, M., Balbous-Gautier, A., Fernagut, P.-O., et al. (2024). Dysfunction of striatal parvalbumin interneurons drives motor stereotypies in Cntnap2−/− mouse model of autism spectrum disorders. *PNAS Nexus* 3:pgae132. doi: 10.1093/pnasnexus/pgae132

Tisch, S., Silberstein, P., Limousin-Dowsey, P., and Jahanshahi, M. (2004). The basal ganglia: anatomy, physiology, and pharmacology. *Psychiatr. Clin. North Am.* 27, 757–799. doi: 10.1016/j.psc.2004.06.004

Todtenkopf, M. S., Stellar, J. R., Williams, E. A., and Zahm, D. S. (2004). Differential distribution of parvalbumin immunoreactive neurons in the striatum of cocaine sensitized rats. *Neuroscience* 127, 35–42. doi: 10.1016/j.neuroscience.2004.04.054

Vinnakota, C., Hudson, M. R., Jones, N. C., Sundram, S., and Hill, R. A. (2023). Potential roles for the GluN2D NMDA receptor subunit in schizophrenia. *Int. J. Mol. Sci.* 24:11835. doi: 10.3390/ijms241411835

Wang, X., Gallegos, D. A., Pogorelov, V. M., O'Hare, J. K., Calakos, N., Wetsel, W. C., et al. (2018). Parvalbumin interneurons of the mouse nucleus Accumbens are required for amphetamine-induced locomotor sensitization and conditioned place preference. *Neuropsychopharmacology* 43, 953–963. doi: 10.1038/npp.2017.178

Wang, W. X., Qiao, J., and Lefebvre, J. L. (2022). PV-IRES-Cre mouse line targets excitatory granule neurons in the cerebellum. *Mol. Brain* 15:85. doi: 10.1186/s13041-022-00972-1

Wiltschko, A. B., Pettibone, J. R., and Berke, J. D. (2010). Opposite effects of stimulant and antipsychotic drugs on striatal fast-spiking interneurons. *Neuropsychopharmacology* 35, 1261–1270. doi: 10.1038/npp.2009.226

Wingert, J. C., and Sorg, B. A. (2021). Impact of Perineuronal nets on electrophysiology of Parvalbumin interneurons, principal neurons, and brain oscillations: a review. *Front Synaptic Neurosci* 13:673210. doi: 10.3389/fnsyn.2021.673210

Yamada, H., Inokawa, H., Hori, Y., Pan, X., Matsuzaki, R., Nakamura, K., et al. (2016). Characteristics of fast-spiking neurons in the striatum of behaving monkeys. *Neurosci. Res.* 105, 2–18. doi: 10.1016/j.neures.2015.10.003

Zhou, X., Wu, B., Liu, W., Xiao, Q., He, W., Zhou, Y., et al. (2021). Reduced firing of nucleus Accumbens Parvalbumin interneurons impairs risk avoidance in DISC1 transgenic mice. *Neurosci. Bull.* 37, 1325–1338. doi: 10.1007/s12264-021-00731-7